Quantitative Modeling of Membrane Deformations by Multihelical Membrane Proteins: Application to G-Protein Coupled Receptors

Sayan Mondal,[†] George Khelashvili,[†] Jufang Shan,[†] Olaf S. Andersen,[†] and Harel Weinstein[†‡*]

[†]Department of Physiology and Biophysics and [‡]The HRH Prince Alwaleed Bin Talal Bin Abdulaziz Alsaud Institute for Computational Biomedicine, Weill Medical College of Cornell University, New York, New York

ABSTRACT   The interpretation of experimental observations of the dependence of membrane protein function on the properties of the lipid membrane environment calls for a consideration of the energy cost of protein-bilayer interactions, including the protein-bilayer hydrophobic mismatch. We present a novel (to our knowledge) multiscale computational approach for quantifying the hydrophobic mismatch-driven remodeling of membrane bilayers by multihelical membrane proteins. The method accounts for both the membrane remodeling energy and the energy contribution from any partial (incomplete) alleviation of the hydrophobic mismatch by membrane remodeling. Overcoming previous limitations, it allows for radially asymmetric bilayer deformations produced by multihelical proteins, and takes into account the irregular membrane-protein boundaries. The approach is illustrated by application to two G-protein coupled receptors: rhodopsin in bilayers of different thickness, and the serotonin 5-HT$_{2A}$ receptor bound to pharmacologically different ligands. Analysis of the results identifies the residual exposure that is not alleviated by bilayer adaptation, and its quantification at specific transmembrane segments is shown to predict favorable contact interfaces in oligomeric arrays. In addition, our results suggest how distinct ligand-induced conformations of G-protein coupled receptors may elicit different functional responses through differential effects on the membrane environment.

INTRODUCTION

Many aspects of the function and organization of multihelical membrane proteins, such as G-protein coupled receptors (GPCRs), depend on their lipid membrane environment (1–7). For example, flash photolysis and NMR experiments show that the photochemical function of the GPCR rhodopsin is affected by the lipid bilayer composition (1,8). Fluorescence resonance energy transfer (FRET) experiments (9) and coarse-grained molecular-dynamics (MD) simulations (10) suggest that rhodopsin oligomerizes to different extents in monounsaturated phosphatidylcholine (PC) membranes of different thickness. Such observations have been rationalized largely in terms of the energy cost of membrane deformations due to hydrophobic mismatch, i.e., the difference between the hydrophobic thickness of the unperturbed membrane and the hydrophobic length of the membrane-embedded protein (11–14). In the presence of a hydrophobic mismatch, the membrane deforms to alleviate the energetically costly exposure of hydrophobic residues (11–13), which incurs an energy penalty. If an incomplete hydrophobic adaptation occurs, an additional energy contribution will be made to the energy penalty (15–17). Such incomplete adaptation has been inferred from EPR studies on lipid-protein interactions for a number of multihelical proteins (16).

One can evaluate the membrane remodeling due to hydrophobic mismatch, and its associated energy cost, by approximating the lipid bilayer as an elastic continuum (12,13). With the energy functional comprising compression-extension, curvature, and surface tension terms, the theory of elastic membrane deformations can quantitatively explain the effect of bilayer thickness on the lifetime of the gramicidin ion channels (12,13,15). The continuum theory is usually implemented with the simplifying assumption of radially symmetric membrane deformation, which is reasonable for single helical proteins such as the gramicidin channel. However, for multihelical proteins such as GPCRs, where the transmembrane (TM) segments have different hydrophobic lengths and the membrane must adapt to different heights along the protein-lipid boundary, the membrane deformation will be radially asymmetric. Moreover, the extent to which a particular TM segment is buried in the lipid membrane will depend not only on the hydrophobic length of that segment and the thickness of the bilayer but also on the constraints imposed by the need to reduce the hydrophobic mismatch at the adjacent TM segments and the local conformation of the side chains.

We therefore reasoned that a new approach to quantify the hydrophobic mismatch-driven bilayer remodeling and its energetics for inserted multihelical membrane proteins was necessary to account for the interaction of multi-TM proteins with the phospholipid bilayer. The method presented here achieves this goal by combining the elastic theory of membrane deformations with atomistic MD simulations. We incorporate the consequences of the different hydrophobic mismatches for different TM segments in multihelical proteins by using MD simulations, which makes it

Editor: Lukas Tamm.

possible to evaluate the radially asymmetric remodeling of the membrane around the protein equilibrated in its environment. This approach allows us to quantify the surface area of residues exposed to unfavorable hydrophobic-polar interactions between the lipid and the protein at specific TM segments (termed residual exposure), and calculate the corresponding energy penalty.

Here we present the methodological details of the approach and illustrate its implementation using results for two different GPCRs inserted into membranes of various lipid compositions. We use five different systems to compare rhodopsin immersed in monounsaturated PC membranes of different thicknesses: 1), $diC_{14:1}PC$; 2), $diC_{16:1}PC$; 3), $diC_{18:1}PC$; 4), $diC_{20:1}PC$; and 5), a bilayer composed of a 7:7:6 mixture of $1-C_{18:0}-2-C_{22:6}-PC$ (SDPC), $1-C_{16:0}-2-C_{18:1}-PC$ (POPC), and cholesterol (Chol). In addition, we use three systems to compare the serotonin $5-HT_{2A}$ receptor ($5HT_{2A}R$) complexed with pharmacologically different ligands: 1), the agonist serotonin (5-HT); 3), the partial agonist (LSD); and 3), the inverse agonist ketanserin (KET) immersed in the 7:7:6 SDPC/POPC/Chol membrane.

We show that the energy values obtained for the membrane deformation and membrane-protein interaction identify an energy-based mechanism for reduction of the residual exposure at specific TM domains by oligomerization of multi-TM membrane proteins. For investigations of hydrophobic mismatch-driven oligomerization, such results should aid researchers in predicting putative oligomerization interfaces based on results from atomistic simulations of the monomers.

THEORY AND METHODS

Multiscale description of protein-membrane complexes

The formalism introduced here describes the protein-remodeled bilayer shape in three dimensions by combining macroscopic continuum-level (CT) calculations with results from cognate MD simulations. We denote this procedure 3D-CTMD, for three-dimensional combined continuum and MD.

The framework is developed for integral membrane proteins comprising N_{TM} TM segments embedded in a lipid membrane. We use a rhodopsin-like GPCR ($N_{TM} = 7$) to illustrate the method, which is generally applicable to multihelical proteins. The membrane-inserted segments can have different hydrophobic lengths, with L_i denoting the projected hydrophobic length along the membrane normal. In general, the L_i-values will not match the hydrophobic thickness of the unperturbed membrane, d_0, and the formulation allows for proteins with different L_i-values for each TM segment, thus allowing for radial variation of the hydrophobic mismatch. Importantly, the formalism is also able to account for residual hydrophobic exposure and hydrophobic slippage, i.e., situations in which the energetic cost of locally adapting the membrane lipids to the protein precludes complete alleviation of the hydrophobic mismatch by means of membrane deformation alone.

The starting point for the calculations is a well-converged, explicit-solvent, all-atom MD trajectory of a monomer of the GPCR embedded in the lipid membrane of interest (for details, see Supporting Material). The MD simulations provide information about the organization of the protein in the membrane and the interfacial protein/lipid interactions in the MD-equilibrated state of the protein with the bilayer adopting the energetically most favorable shape around the GPCR. In this state, both the protein conformation and the hydrophobic adaptation are assumed to be energetically optimal with respect to the compensation between the energetic cost of the residual hydrophobic exposure, the membrane deformation, and any reorganization of the protein. This assumption is used to guide the parameterization of the protein-lipid interfacial interactions at the CT level in the transition from atomistic to continuum description. In the CT representation, the TM protein is described in terms of 1), the L_i-values of the constituent TM segments; 2), the contour Γ_{in} of the protein boundary within the surrounding membrane; and 3), the membrane thickness u_0 at this boundary. These geometric measures are taken from the structure (averaged over the last 100 ns of the converged trajectory in the MD simulation) of the GPCR-membrane system (see Supporting Material).

The membrane shape is described by the local deformation variable $u(x,y)$, defined as

$$u(x, y) = \frac{1}{2}(d(x, y) - d_0), \qquad (1)$$

where $d(x,y)$ and d_0 are the local and bulk bilayer thicknesses, respectively. This definition maintains the simple representation used in previous work (13) by effectively taking the average of the deformations in the two leaflets of the bilayer (we verified that treating the two leaflets separately does not affect the results for the GPCR systems studied here).

Free-energy cost of the hydrophobic mismatch

The CTMD method addresses both key contributions to the hydrophobic mismatch energy penalty, i.e., the membrane-deformation energy penalty ΔG_{def} and the residual hydrophobic exposure energy penalty ΔG_{res} (16).

ΔG_{def} in the system equilibrated with MD using the theory of elastic bilayer deformations, with contributions from compression-extension, splay-distortion, and surface tension terms (13):

$$\Delta G_{def} = \frac{1}{2} \int_{\Omega} \left\{ K_a \frac{(2u)^2}{d_0^2} + K_c \left(\frac{\partial^2 u}{\partial x^2} + \frac{\partial^2 u}{\partial y^2} - C_o \right)^2 \right. \\ \left. + \alpha \left(\left(\frac{\partial u}{\partial x} \right)^2 + \left(\frac{\partial u}{\partial y} \right)^2 \right) \right\} d\Omega, \qquad (2)$$

where K_c and K_a are the elastic moduli for splay-distortion and compression-extension respectively; C_0 represents the monolayer spontaneous curvature; and α denotes the surface tension. The free-energy expansion in Eq. 2 is valid for small deformations relative to the monolayer thickness, which is the case for the GPCR-membrane systems studied here (see Table S1 and Fig. 2 and Fig. S7).

The residual exposure energy penalty ΔG_{res} arises from any incomplete alleviation of hydrophobic mismatch due to the high energy cost that such a membrane deformation might entail, and penalizes the unfavorable hydrophobic-hydrophilic interactions at the protein-lipid interface in the equilibrated system. This energy penalty can be approximated as being linearly proportional to the unfavorably exposed surface area at the protein-membrane interface (17–19), in which case ΔG_{res} is the sum of the residual energies at each TM:

$$\Delta G_{res} = \sum_{i=1}^{N_{TM}} \Delta G_{res,i} \sim \sum_{i=1}^{N_{TM}} \sigma_{res} SA_{res,i}, \qquad (3)$$

where $SA_{res,i}$ is the exposed surface area of the ith TM, as estimated from the MD trajectories, and σ_{res} is taken to be 0.028 kcal/(mol. $\mathring{A}^2$), the value estimated from the transfer energies of peptide residues between hydrophobic and polar environments (18,19).

Calculation of equilibrium membrane shapes and ΔG_{def} from free-energy minimization

The time-averaged $u(x,y)$ derived from MD data is not directly used to calculate the ΔG_{def} from Eq. 2 because it is constructed from the discrete phosphate positions of the MD trajectory and hence is too noisy for direct numerical calculation of the second derivatives in the curvature term of the continuum-level free-energy expression in Eq. 2. Instead, we determine the equilibrium $u(x,y)$ from continuum-level macroscopic calculations by self-consistently minimizing the ΔG_{def} given in Eq. 2, subject to boundary conditions provided by the MD simulations. For the minimization, we use the Euler-Lagrange formulation, solving the following boundary value problem (13):

$$K_C \nabla^4 u - \alpha \nabla^2 u + \frac{4K_a}{d_0^2} u = 0,$$
$$u|_{\Gamma_{in}} = u_o(x,y), u|_{\Gamma_{out}} = 0, \nabla^2 u|_{\Gamma_{in}} = \nu_o(x,y), \nabla^2 u|_{\Gamma_{out}} = 0,$$
$$(4)$$

where the symbols Γ_{in} and Γ_{out} denote the boundary at the protein-membrane interface and the outer boundary of the simulation box, respectively. We obtain the Γ_{in} and Γ_{out} values and the boundary condition $u_O(x,y)$ from the MD simulations, and, consistent with current practice (15,16), we use bulk elastic moduli to describe the bilayer close to the protein-bilayer boundary in the calculations of ΔG_{def}. We solve Eq. 4 using a finite-difference scheme, with the boundary condition on the membrane curvature at the protein-lipid interface, $v_o(x,y)$, obtained self-consistently from an optimization procedure (see Supporting Material for details). Here, $v_o(x,y)$ is the asymmetric generalization of the so-called natural boundary condition (20), which has been shown to work well (21) and is the most straightforward to use in the mathematical algorithm presented here (see Supporting Material). Importantly, this formalism does not invoke symmetry at the membrane-protein boundary Γ_{in} or in membrane deformations $u(x,y)$; rather, it treats Γ_{in} as an irregular contour, thus allowing for radially asymmetric changes in membrane shape. Fig. 1 illustrates the protocol for rhodopsin in a diC$_{14:1}$PC bilayer. ΔG_{def} is obtained from the $u(x,y)$ thus calculated.

In this framework for calculating ΔG_{def}, the boundary condition from MD provides the pattern of local membrane deformation at the lipid-protein interface, taking into account at the atomistic level the equilibrated structure of the protein in the membrane and the various interactions within the protein-membrane system. Importantly, this strategy incorporates the effect of the radially asymmetric and irregular hydrophobic surface of the protein involved in membrane-protein interactions. Consequently, the self-consistent determination of $u(x,y)$ using Eq. 4 is not only a numerically viable solution for calculating ΔG_{def} using the well-tested elastic continuum theory of membrane deformations, it also yields the macroscopic $u(x,y)$ (with ΔG_{def} defined by Eq. 2) that is directly comparable to the $u(x,y)$ obtained from the cognate microscopic MD simulation.

Residual hydrophobic exposure energies

The residual exposure energy ΔG_{res} is obtained as described in Eq. 3. The residual exposure area $SA_{res,i}$ at the ith TM is determined using the solvent-accessible surface areas (SASA) of the relevant residues from the MD trajectories (see Supporting Material for details).

RESULTS

Using our 3D-CTMD approach, we obtained quantitative descriptions of the hydrophobic mismatch-based remodeling of the membrane surrounding multihelical proteins in the rhodopsin-like GPCR class: a rhodopsin monomer
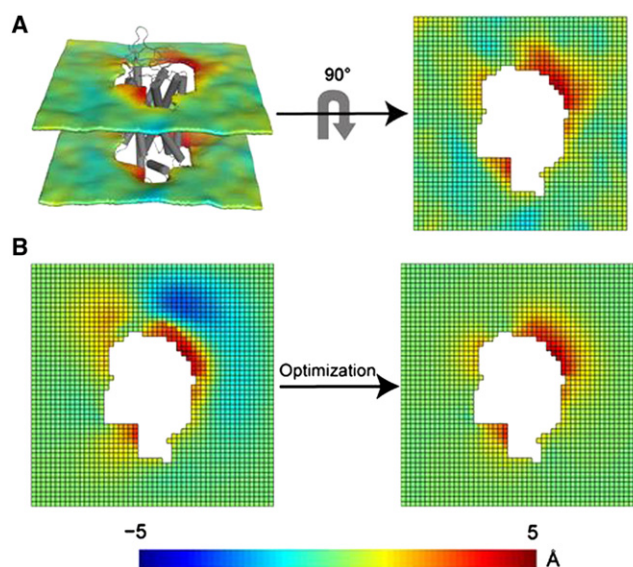
FIGURE 1 Protocol for the 3D-CTMD approach, illustrated for rhodopsin in a diC$_{14:1}$PC lipid bilayer. (*A*) The membrane-deformation profile $u(x,y)$ calculated directly from the MD simulations. The left panel is the deformation profile as a color map projected onto the surface defined by fitting a grid (spacing 2 Å) to the positions of the phosphate atoms in the two leaflets during the trajectory, followed by time averaging and spatial smoothing. The right panel shows the same deformation color map on the *x-y* plane. (*B*) The membrane-deformation profile $u(x,y)$ on a 100 × 100 Å patch, calculated with 3D-CTMD. The left panel represents the membrane shape calculated with the deformation boundary condition at the membrane-protein interface from the MD profile in panel *A* and a random curvature boundary condition to produce the starting point for the free-energy-based optimization (Eqs. S2 and S3). The right panel is the membrane-deformation profile calculated with the natural boundary condition, which minimizes the membrane-deformation energy penalty. Note the agreement between the profiles in *A*, calculated using a microscopic theory, and *B*, calculated using the continuum theory (they are within 0.5 Å RMSD of each other). The 3D-CTMD approach also allows evaluation of the protein-induced membrane-deformation energy penalty, which is 4.7 *kT* in this case.

immersed in lipid membranes of different bulk thicknesses, and a serotonin 5-HT$_{2A}$R monomer binding three different ligands known to have different pharmacological efficacies (i.e., the agonist 5-HT, the partial agonist LSD, and the inverse agonist KET) immersed in an SDPC/POPC/Chol membrane model.

For each construct, the 3D-CTMD method was used to calculate the membrane-deformation profile $u(x,y)$ as well as the contributions from the membrane deformation ΔG_{def} and the residual hydrophobic exposure ΔG_{res} to the energy penalty due to hydrophobic mismatch (see Theory and Methods, and Fig. 1 *B*), in the context of the MD trajectories of the systems.

Membrane remodeling by rhodopsin depends on lipid composition and is radially asymmetric

Fig. 2 shows the membrane-deformation profiles $u(x,y)$ and the corresponding membrane-deformation energy ΔG_{def} for
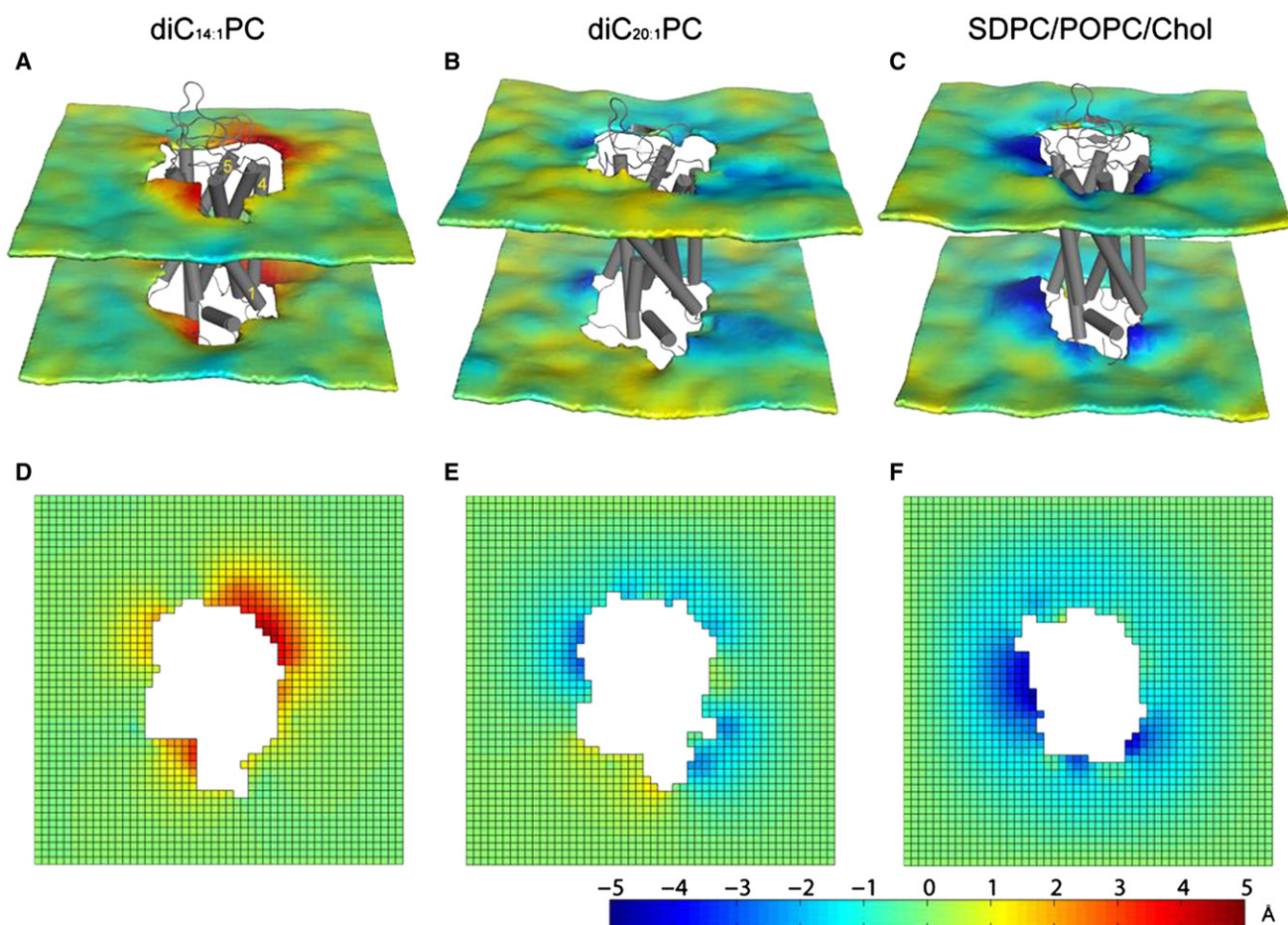
FIGURE 2 Membrane-deformation profiles $u(x,y)$ for rhodopsin immersed in lipid bilayers of different bulk thicknesses. The upper panel shows $u(x,y)$ calculated directly from MD trajectories for rhodopsin in bilayers composed of (A) $diC_{14:1}PC$, (B) $diC_{20:1}PC$, and (C) 7:7:6 SDPC/POPC/Chol membranes. The lower panel shows the corresponding membrane-deformation profiles $u(x,y)$ for (D) $diC_{14:1}PC$, (E) $diC_{20:1}PC$, and (F) 7:7:6 SDPC/POPC/Chol calculated using the 3D-CTMD approach. The corresponding membrane-deformation energies ΔG_{def} are (D) 4.7 k_BT, (E) 2 k_BT, and (F) 2.6 k_BT. The calculated ΔG_{def} is 1.6 kT for rhodopsin in $diC_{16:1}PC$, and 0.8 kT for rhodopsin in $diC_{18:1}PC$.

rhodopsin in $diC_{14:1}PC$, $diC_{20:1}PC$, and 7:7:6 SDPC/POPC/Chol membranes. The $u(x,y)$ profile obtained from 3D-CTMD (*lower panel*) shows good agreement with the time-averaged $u(x,y)$ constructed directly from the MD (*upper panel*; root mean-square difference (RMSD) ~10% of the range of deformations; difference color maps are shown in Fig. S3).

The average membrane deformations near the rhodopsin (averaged over the bilayer region within 12 Å of the $C\alpha$ atoms of the protein, which corresponds to one lipid shell around the protein) are small (the maximum being ~2–2.5 Å in $diC_{14:1}PC$ and SDPC/POPC/Chol; see Table S1). This finding agrees with findings from solid-state NMR experiments on rhodopsin reconstituted in $1-C_{n:0}-2-C_{n:1}$-PC bilayers of different tail lengths at the molar ratio of 1:250 (22). From these experiments, the 14-C tail bilayer was inferred to deform by ~2 Å in the first lipid shell around the protein, and the 16-C, 18-C, and 20-C tail bilayers were inferred to deform by <0.5 Å (22). As expected from the

varying L_i (Table S2 and Table S3), the deformations we calculate are radially asymmetric, and the various membranes show substantial local thickening and thinning (Fig. 2). For example, in the $diC_{14:1}PC$ bilayer, the membrane thickens by ~5 Å near TM4, even though the average thickness change is only ~2 Å around the entire TM bundle. The values for ΔG_{def} in the different systems are listed in the legend of Fig. 2 and in Table S1. Note that the usual assumption of radial symmetry would underestimate ΔG_{def}. For example, calculations for $diC_{14:1}PC$ that were predicated on the assumption of radial symmetry, obtained within the CTMD approach by setting the membrane deformation at all points on the protein-membrane boundary uniformly to the value of the average membrane deformation near the protein, yielded ~1.9 kT (for details, see Supporting Material). This result contrasts with the 4.7 kT obtained without the assumption of radial symmetry.

Overall, the thicker bilayers ($diC_{20:1}PC$ and 7:7:6 SDPC/POPC/Chol) become thinner near the protein, whereas the

thinner bilayers (diC$_{14:1}$PC and diC$_{16:1}$PC) become thicker locally around the protein. These trends suggest that, as expected, the membrane deformation around the TM segments tends to alleviate the mismatch between the protein's hydrophobic length and the bilayer's hydrophobic thickness. Fig. 3 demonstrates a particular instance of such hydrophobic adaptation, which taken together with Fig. 2 B suggests that the diC$_{20:1}$PC bilayer thins near TM5 to prevent residue Glu-201(5.36) from being embedded in the hydrophobic core (the residue number in parentheses is given in the Ballesteros-Weinstein generic system (23) to identify the position in the TM).

Yet, the mismatch is only partially alleviated by the membrane deformation, leaving a substantial residual hydrophobic exposure at specific TM segments in all the simulated systems (Table 1 and Fig. 3).

The residual exposure energy penalty varies among TM segments

To calculate the energy cost of the residual hydrophobic exposure ΔG_{res}, we identified the residues that contributed to the residual penalty in each TM from the MD trajectories. The SASAs of these residues were calculated (see Supporting Material for details) to obtain the residual surface area $SA_{res,i}$ for the ith TM segment as the sum of the SASAs for the unfavorably exposed side chains (and methylene groups). We tested the effect of the SASA definition by changing the probe radius for these calculations from the standard value of 1.4 Å, to 1.2 Å, which changed the calculated residual exposure at the different TM segments by only 0–10 Å^2 (which corresponds to $< \sim 0.5$ kT). The calculated $SA_{res,i}$ values were used to compute the corresponding
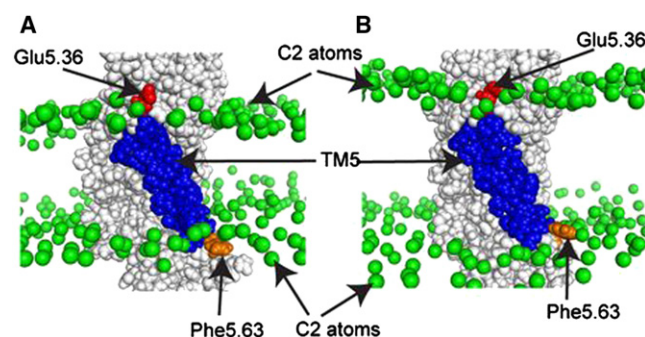

FIGURE 3 Illustration of hydrophobic adaptation and residual exposure at the molecular level. (A) A snapshot from the MD trajectory of rhodopsin in the thin diC$_{14:1}$PC bilayer. TM5 is shown in blue, and two residues (Glu-5.36 and Phe-5.63) are highlighted. (B) A snapshot of rhodopsin in the thick diC$_{20:1}$PC bilayer. The diC$_{20:1}$PC bilayer thins near Glu-5.36, which substantially reduces its exposure to the hydrophobic core of the bilayer, thus showing hydrophobic adaptation. Phe-5.63 remains unfavorably exposed to the polar environment in the thin diC$_{14:1}$PC bilayer but not in the thick diC$_{20:1}$PC bilayer. Thus, Phe-5.63 contributes to residual exposure energy penalty at TM5 for rhodopsin in diC$_{14:1}$PC. The residual exposures are computed over the course of the MD trajectory (Table 1).

$\Delta G_{res,i}$ from Eq. 3. $\Delta G_{res,i}$ penalizes both hydrophilic residues of the protein exposed to the hydrophobic core of the lipid environment, and hydrophobic residues of the protein exposed to polar environment.

Table 1 lists the $SA_{res,i}$ and $\Delta G_{res,i}$ values for rhodopsin TM segments in all of the simulated membranes. $\Delta G_{res,i}$ varies substantially among the TM segments and, for each segment, among the different bilayers. In particular, $\Delta G_{res,4}$ increases from a value of 0 in the thin diC$_{14:1}$PC membranes to 6.3 $k_B T$ in the thick SDPC/POPC/Chol membranes. In contrast, $\Delta G_{res,i}$ for TM1, TM2, and TM7 decreases from the thinner to the thicker membranes. The mismatch at TM5 appears to be alleviated in the bilayers composed of 16:1 or longer lipid tails, because $\Delta G_{res,5}$ is effectively zero in all of the systems except diC$_{14:1}$PC, where it is 5.4 $k_B T$. As an example, the residual exposure at TM5 is illustrated in Fig. 3 A, which shows that the hydrophobic residue Phe-228(5.63) is exposed to the polar environment in the thin diC$_{14:1}$PC but not in diC$_{20:1}$PC. Finally, the results in Table 1 show that the hydrophobic mismatch is most effectively alleviated, with the overall $\Delta G_{res,i}$ being smallest, in diC$_{20:1}$PC membranes. As noted in the Discussion, the results from these calculations identify likely interfaces in any hydrophobic mismatch-driven oligomerization of the GPCR.

The ligand-dependent activation states of the 5-HT$_{2A}$ receptor determine membrane remodeling

We recently showed how ligands with different pharmacological properties (i.e., full, partial, and inverse agonists) stabilize different conformations of the serotonin 5-HT$_{2A}$ receptor (24). Here we show that these different ligands also alter the pattern of membrane deformation and the residual hydrophobic exposure energy penalties around their host receptor. For the 3D-CTMD calculations, we used the 350 ns long MD simulations of the 5-HT$_{2A}$R in complex with either the full agonist 5-HT, the partial agonist LSD, or the inverse agonist KET (24). The differential conformational changes in response to ligand binding revealed by the atomic-level simulations of the bound GPCR in 7:7:6 SDPC/POPC/Chol membranes are reflected in distinct rigid-body rearrangements of TM1, TM4, and TM6 (24).

The results from the 3D-CTMD calculations reveal a distinct pattern of bilayer deformations around 5-HT$_{2A}$R for the different bound ligands. The largest membrane thinning is observed around TM1 in the KET simulation, and around TM6 in the 5-HT simulation (Fig. S7). The bilayer deformations around TM4 are larger with LSD or 5-HT than with KET bound. The residual hydrophobic exposure energies of the TM segments in the three systems differ as well (Table 2). There is a substantial residual penalty (~ 5 $k_B T$) for TM1, but only in the KET-bound GPCR; the residual penalty for TM6 is nonzero only in the 5-HT-bound system. Table 2 further shows that the residual penalty for

TABLE 1 Residual SA_{res} values (in Å^2) and the corresponding ΔG_{res} values (in $k_B T$) calculated for TMs of rhodopsin in diC$_{14:1}$PC, diC$_{16:1}$PC, diC$_{18:1}$PC, diC$_{20:1}$PC, and 7:7:6 SDPC/POPC/Chol membranes

TM	diC$_{14:1}$PC		diC$_{16:1}$PC		diC$_{18:1}$PC		diC$_{20:1}$PC		SDPC/POPC/Chol	
	SA_{res}	ΔG_{res}	SA_{res}	ΔG_{res}	SA_{res}	ΔG_{res}	SA_{res}	ΔG_{res}	SA_{res}	ΔG_{res}
1	210	9.9	80	3.8	75	3.5	70	3.3	63	3.0
2	74	3.5	29	1.4	0	0	32	1.5	27	1.3
3	N.D.	N.D.	N.D.	N.D.	N.D.	N.D.	N.D.	N.D.	N.D.	N.D.
4	0	0	77	3.6	90	4.3	79	3.7	134	6.3
5	115	5.4	1	0	9	0.4	7	0.3	17	0.8
6	36	1.7	31	1.5	56	2.7	38	1.8	51	2.4
7	119	5.6	44	2.1	22	1.1	0	0	0	0

SA_{res} values were calculated by using the SASA-based method (see Theory and Methods) with a probe radius of 1.4 Å. Probes with smaller radii did not significantly change the SA_{res} estimates. N.D., not determined.

TM4 increases in the order 5-HT < LSD < KET, and that the penalty for TM5 decreases with the same rank order. Taken together with the results from the cognate MD simulations, showing differential movement of TM1, TM4, and TM6 (24), our 3D-CTMD formalism provides a quantitative link between the different perturbations of the GPCR structure produced by the binding of pharmacologically distinct ligands, and the energetics of unfavorable residual hydrophobic exposure of the receptor in complexes. As discussed below, these quantitative findings suggest a mechanistic explanation for differential interfaces in ligand-driven oligomerization of the GPCRs.

DISCUSSION

To quantify the membrane deformations due to hydrophobic mismatch, and the associated energy cost, we used atomistic MD simulations together with the framework provided by the theory of elastic membrane deformations (12,13) in which the energy functional comprises compression-extension, splay-distortion, and surface-tension terms. The theory of elastic bilayer deformations has been used to account quantitatively for the lifetime variations of gramicidin channels in membranes of different thicknesses (12,15), and for the lateral dimerization of gramicidin channel constructs

TABLE 2 Residual SA_{res} values (in Å^2) and corresponding ΔG_{res} values (in $k_B T$) calculated for TMs of 5-HT$_{2A}$R in complex with 5-HT, LSD, and KET, respectively, in an SDPC/POPC/Chol lipid bilayer

TM	5-HT$_{2A}$R with 5-HT		5-HT$_{2A}$R with LSD		5-HT$_{2A}$R with KET	
	SA_{res}	ΔG_{res}	SA_{res}	ΔG_{res}	SA_{res}	ΔG_{res}
1	0	0	0	0	107	5.1
2	30	1.4	0	0	0	0
3	N.D.	N.D.	N.D.	N.D.	N.D.	N.D.
4	25	1.2	81	3.8	103	4.9
5	94	4.4	81	3.8	69	3.3
6	40	1.9	0	0	0	0
7	1	0	0	0	0	0

SA_{res} values were calculated by using the SASA-based method (see Theory and Methods) with a probe radius of 1.4 Å. Probes with smaller radii did not significantly change the SA_{res} estimates. N.D., not determined.

comprising pairs of gramicidin subunits tethered with peptide linkers (14,25). In these studies, the gramicidin channels were assumed to be cylindrical, which is reasonable for a single-segment TM protein. In the case of more-complex proteins, such as multihelical GPCRs with TM segments of different hydrophobic thickness, calculations of membrane remodeling and the associated energetics require a representation of the membrane deformation that allows for radial asymmetry. We accomplished this with our multiscale 3D-CTMD approach, which combines information about the membrane thickness at the protein-lipid interface from atomistic MD simulations with the continuum formalism in an energy functional comprising compression-extension, curvature, and surface-tension terms.

We are aware of only one other study in which a combined MD and continuum approach was used to calculate the protein-induced membrane deformation in three dimensions, which was applied to the gating of mechanosensitive channels. In that work, Chen et al. (26) parametrized the continuum calculations using a coarse-grained, implicit-solvent, implicit-membrane MD simulation of a single helix-membrane system. In our 3D-CTMD approach, we overcome some of the limitations of the former approach. First, we determine the asymmetric membrane thickness boundary condition around the multisegment protein from atomistic MD simulations, which allows for asymmetric membrane-deformation profiles. Second, we consider the residual hydrophobic exposure and the corresponding energy cost at each TM segment (thus enabling an evaluation of localized contributions of the hydrophobic mismatch energies in membrane-mediated protein-protein interactions).

Application of the 3D-CTMD framework to membranes containing multisegment GPCR proteins yields patterns of deformation that are radially asymmetric and dependent on lipid composition, in agreement with earlier observations from coarse-grained MD simulations (10). The deformed membrane shapes calculated with the 3D-CTMD method are in excellent agreement with the smoothed membrane shape obtained from atomistic MD simulations (Figs. 1 and 2 and Fig. S7). This observation is consistent with the generally held view that molecular approaches and

continuum elastic approaches should yield similar results at length scales comparable to the membrane thickness (27). The important advantage of obtaining the membrane-deformation profile from the 3D-CTMD approach, rather than directly from MD, is that it allows us to also evaluate the energy cost of the membrane deformation. In our recent study of a single helical membrane-inserting peptide (Dynorphin A), we found that the self-consistent solution to Eq. 4 agreed well with the deformation profile predicted from MD for liquid-disordered membrane systems but not for liquid-ordered systems. This could be due to limitations in Eq. 4 in accounting for the constraints on lipid packing at the membrane-protein boundary (28–31). We also showed that introducing the boundary conditions from the MD simulation, instead of a self-consistent solution procedure, solved this problem (32).

Our results identify ΔG_{res} as a substantial energy component in GPCR-membrane systems, in general agreement with inferences from lipid association studies of various multihelical TM proteins (16). In these systems, the bilayer deformation fails to completely alleviate the hydrophobic mismatch around the protein due to the different hydrophobicity lengths and patterns of adjacent TM segment. Rather, the membrane deforms to an extent that minimizes the total energy cost due to hydrophobic mismatch, as can be deduced by uniformly varying the bilayer thickness at all points on the membrane-protein boundary in steps of 0.5 Å for the different systems (Fig. S6). The results show that 1), the total residual exposure decreases linearly with increasing membrane deformation; 2), the membrane-deformation energy increases quadratically with increasing membrane deformation; and 3), the minimum in the total energy occurs within ± 0.5 Å of the MD-derived boundary condition for the different systems. Furthermore, unlike single-helical peptides such as the gramicidin channels, the hydrophobic mismatch of multihelical proteins such as the GPCRs exhibits substantial local variation due to the different hydrophobic lengths of the TM segments (see Table S2 and Table S3). Therefore, completely alleviating the hydrophobic mismatch at all loci by just deforming the membrane would be energetically prohibitive because it would require large slopes (and curvatures) of the deformation profile between adjacent segments. Indeed, whenever adjacent TM segments are out of register (meaning that the positions of their hydrophobic/hydrophilic boundaries differ sufficiently to prevent a membrane lipid molecule from hydrophobically adapting to both segments), a residual hydrophobic exposure, with its associated energetic cost, will occur. Not surprisingly, therefore, the helix packing varies when the bilayer thickness is varied, as indicated by a comparison of the panels in Fig. 2 showing the results of the MD simulations.

This residual hydrophobic exposure can occur even if the protein's average hydrophobic length is equal to the average thickness of the unperturbed bilayer. Thus, the hydrophobic

exposure is more than the hydrophobic slippage that arises when the incremental increase in ΔG_{def} becomes larger than the incremental energetic cost of exposing hydrophobic residues to a polar environment (15). By applying the 3D-CTMD approach to the 5-HT$_{2A}$ receptor complexed with pharmacologically distinct GPCR ligands (24), we found that the structurally distinct complexes obtained from the MD simulations were surrounded by different patterns of membrane deformations and hence generated different values of protein-membrane interaction energies. In particular, our 3D-CTMD calculations identify quantitatively, for the first time to our knowledge, the substantial residual exposures at some TM segments of the 5-HT$_{2A}$ receptor models due to the incomplete alleviation of the hydrophobic mismatch, and their dependence on membrane composition and protein structure.

As we discuss below, the energetic cost of the local, residual hydrophobic exposure at specific TM segments can be reduced (or eliminated) by the participation of the segments in interfaces between different protomers in oligomeric constructs. Indeed, the calculated residual energy penalties were found to vary in different lipid membranes, at different segments, and for the conformation achieved by the same GPCR with different ligands in the binding site. It is therefore reasonable to suggest that bringing together in the membrane the TM segments from separate protomers that were calculated to incur the highest energy penalty from residual hydrophobic exposure could be a significant component of the energetic drive for oligomerization. In such a mismatch- or exposure-driven oligomerization model, the quantitative findings presented here should have implications for the mechanistic description of GPCR oligomerization and for predicting oligomeric interfaces, taking into consideration both ligand-specific conformations and membrane properties, as discussed further below.

Consistent with current practice (13,16), we calculated ΔG_{def} using bulk elastic moduli to describe the lipid close to the protein-bilayer boundary. If the local moduli were larger than in bulk, due to perturbations of lipid properties by protein-lipid interactions (as suggested previously (33)), our calculations would provide lower bounds for ΔG_{def}, but this would not affect our conclusions. The numerical algorithm of the CTMD framework can be extended to accommodate spatially varying elastic parameters (e.g., as used by Partenskii and Jordan (33)). The major challenge for such an implementation is the need to reliably determine the spatial variation of the elastic parameters. Once such information becomes available, its accommodation within the CTMD framework will refine the calculations.

Hydrophobic mismatch and the oligomeric assembly of rhodopsin

The measured FRET efficiency between rhodopsin molecules reconstituted in lipid membranes of different thickness

was found to decrease with increasing basal membrane thickness (going from $diC_{14:1}PC$ to $diC_{20:1}PC$ membranes) (9). This result suggests a greater extent of rhodopsin oligomerization in the thinner $diC_{14:1}PC$ lipids than in the thicker $diC_{20:1}PC$ lipids (9). Furthermore, coarse-grained MD simulations (10) showed that rhodopsin monomers in $diC_{14:1}PC$ membranes self-assemble into higher-order oligomers but remain mostly monomeric in the $diC_{20:1}PC$ membranes. This agrees with the quantitative results presented here, in that the total energy penalty for embedding rhodopsin is much larger in $diC_{14:1}PC$ membranes (~31 k_BT) than in $diC_{20:1}PC$ membranes (~13 k_BT). Therefore, in agreement with the earlier studies, a mismatch-driven oligomerization model would predict that oligomerization will be more pronounced in $diC_{14:1}PC$ than in $diC_{20:1}PC$ membranes. The 3D-CTMD calculations also quantify the two key components of the hydrophobic mismatch penalty, i.e., the membrane-deformation energy ΔG_{def} and the residual exposure energy ΔG_{res}, and show (see Table S1 and legend to Fig. 2) that although ΔG_{def} can be substantial in the short-tailed $diC_{14:1}PC$ lipid membranes (~4.7 k_BT), it is relatively small (<3 k_BT) for all other rhodopsin-membrane systems.

As an example, the results in Table 1 suggest that for rhodopsin monomers in $diC_{14:1}PC$ membranes, the mismatch-driven oligomerization interface would involve predominantly TM1, and that this would change as a function of membrane thickness. Going from the thinner to the thicker bilayers, oligomerization at TM1 becomes less favorable, whereas oligomerization at TM4 becomes more favorable, and becomes predominant in the native-like SDPC/POPC/Chol bilayers. The role of TM4 and TM1 in the oligomerization of GPCRs, including rhodopsin, has been established for native membranes (34), and we can compare these predictions with results from coarse-grained MD simulations of rhodopsin molecules in different bilayers (10). The density maps produced by Periole et al. (10) for the self-assembly process of rhodopsin monomers into oligomers in different membranes suggest that in $diC_{16:1}PC$ membranes, rhodopsin molecules would be least likely to associate at TM5 and TM2, whereas in $diC_{20:1}PC$ bilayers, the dimerization would be most probable at TM4 and TM1-TM2. Consistent with these results, we obtained low mismatch energies at TM5 (~0 k_BT) and TM2 (1.4 k_BT) in the $diC_{16:1}PC$ bilayer, and the largest residual hydrophobic exposure penalties at TM4 (~3.7 k_BT) and TM1 (~3.3 k_BT) in the $diC_{20:1}PC$ membrane (see Table 1).

Thus, our results from the calculations on rhodopsin in the various membrane environments agree with experimental observations of oligomerization propensities in these environments, and indicate that a large hydrophobic mismatch energy experienced by the monomeric form of the proteins in the lipid membrane can indicate a strong drive for aggregation to occlude the TM segments at which unfavorable interactions are largest. Furthermore, it has

been experimentally demonstrated for single-helical proteins that a single polar residue exposed to the lipid environment in the monomeric form of the peptide can drive its oligomerization in lipid membranes (35).

Hydrophobic mismatch in ligand regulation of 5-HT$_{2A}$R self-assembly

Several experimental studies have suggested ligand-regulated oligomerization of 5-HT$_{2C}$, dopamine D$_2$, and β_2 adrenergic GPCRs (36,37). Here we show that the 3D-CTMD approach applied to serotonin 5-HT$_{2A}$R complexed with the agonist 5-HT, the partial agonist LSD, and the inverse agonist KET identify ΔG_{res} as the dominant contribution to the overall hydrophobic mismatch energy (compare the ΔG_{res} energy values in Table 2 with the membrane remodeling and ΔG_{def} shown in Fig. S7). The largest residual exposure penalties are contributed by different TM segments in the three distinct states of the receptor stabilized by the three ligands (Table 2). Based on these values, the TM segments with the largest drive for mismatch-driven oligomerization are TM5 in 5HT-bound 5-HT$_{2A}$R; TM4 and TM5 in the LSD-bound configuration; and TM4, TM5, and TM1 in KET-bound 5-HT$_{2A}$R. Our identification of TM1, TM4, and TM5 as putative oligomerization interfaces for the ligand-bound serotonin 5-HT$_{2A}$ receptor agrees well with the known identities of the oligomerization interface in a number of GPCR systems (36–39).

SUPPORTING MATERIAL

Additional details and references (40–65) are available at http://www.biophysj.org/biophysj/supplemental/S0006-3495(11)01128-3.

REFERENCES

1. Soubias, O., W. E. Teague, Jr., …, K. Gawrisch. 2010. Contribution of membrane elastic energy to rhodopsin function. *Biophys. J.* 99: 817–824.

2. Andersen, O. S., and R. E. Koeppe, 2nd. 2007. Bilayer thickness and membrane protein function: an energetic perspective. *Annu. Rev. Biophys. Biomol. Struct.* 36:107–130.

3. Lundbaek, J. A., S. A. Collingwood, …, O. S. Andersen. 2010. Lipid bilayer regulation of membrane protein function: gramicidin channels as molecular force probes. *J. R. Soc. Interface.* 7:373–395.

4. Soubias, O., W. E. Teague, and K. Gawrisch. 2006. Evidence for specificity in lipid-rhodopsin interactions. *J. Biol. Chem.* 281:33233–33241.

5. Lundbaek, J. A., P. Birn, …, O. S. Andersen. 2005. Capsaicin regulates voltage-dependent sodium channels by altering lipid bilayer elasticity. *Mol. Pharmacol.* 68:680–689.

6. Brown, M. F., R. L. Thurmond, …, K. Beyer. 2002. Elastic deformation of membrane bilayers probed by deuterium NMR relaxation. *J. Am. Chem. Soc.* 124:8471–8484.

7. Marsh, D. 2008. Protein modulation of lipids, and vice-versa, in membranes. *Biochim. Biophys. Acta.* 1778:1545–1575.

8. Brown, M. F. 1994. Modulation of rhodopsin function by properties of the membrane bilayer. *Chem. Phys. Lipids.* 73:159–180.

9. Botelho, A. V., T. Huber, …, M. F. Brown. 2006. Curvature and hydrophobic forces drive oligomerization and modulate activity of rhodopsin in membranes. *Biophys. J.* 91:4464–4477.

10. Periole, X., T. Huber, …, T. P. Sakmar. 2007. G protein-coupled receptors self-assemble in dynamics simulations of model bilayers. *J. Am. Chem. Soc.* 129:10126–10132.

11. Harroun, T. A., W. T. Heller, …, H. W. Huang. 1999. Experimental evidence for hydrophobic matching and membrane-mediated interactions in lipid bilayers containing gramicidin. *Biophys. J.* 76:937–945.

12. Huang, H. W. 1986. Deformation free energy of bilayer membrane and its effect on gramicidin channel lifetime. *Biophys. J.* 50:1061–1070.

13. Nielsen, C., M. Goulian, and O. S. Andersen. 1998. Energetics of inclusion-induced bilayer deformations. *Biophys. J.* 74:1966–1983.

14. Goforth, R. L., A. K. Chi, …, O. S. Andersen. 2003. Hydrophobic coupling of lipid bilayer energetics to channel function. *J. Gen. Physiol.* 121:477–493.

15. Lundbaek, J. A., and O. S. Andersen. 1999. Spring constants for channel-induced lipid bilayer deformations. Estimates using gramicidin channels. *Biophys. J.* 76:889–895.

16. Marsh, D. 2008. Energetics of hydrophobic matching in lipid-protein interactions. *Biophys. J.* 94:3996–4013.

17. Mouritsen, O. G., and M. Bloom. 1984. Mattress model of lipid-protein interactions in membranes. *Biophys. J.* 46:141–153.

18. Choe, S., K. A. Hecht, and M. Grabe. 2008. A continuum method for determining membrane protein insertion energies and the problem of charged residues. *J. Gen. Physiol.* 131:563–573.

19. Ben-Tal, N., A. Ben-Shaul, …, B. Honig. 1996. Free-energy determinants of α-helix insertion into lipid bilayers. *Biophys. J.* 70:1803–1812.

20. Aranda-Espinoza, H., A. Berman, …, S. Safran. 1996. Interaction between inclusions embedded in membranes. *Biophys. J.* 71:648–656.

21. West, B., F. L. H. Brown, and F. Schmid. 2009. Membrane-protein interactions in a generic coarse-grained model for lipid bilayers. *Biophys. J.* 96:101–115.

22. Soubias, O., S. L. Niu, …, K. Gawrisch. 2008. Lipid-rhodopsin hydrophobic mismatch alters rhodopsin helical content. *J. Am. Chem. Soc.* 130:12465–12471.

23. Ballesteros, J. A., and H. Weinstein. 1995. Integrated methods for the construction of three-dimensional models and computational probing of structure-function relations in G protein-coupled receptors. *Methods Neurosci.* 25:366–428.

24. Shan, J., G. Khelashvili, …, H. Weinstein. 2011. Pharmacologically distinct ligands induce different states of 5-HT2AR and trigger different membrane remodeling: implications for GPCR oligomerization. *Biophys. J.* 100:254.

25. Al-Momani, L., P. Reiss, and U. Koert. 2005. A lipid dependence in the formation of twin ion channels. *Biochem. Biophys. Res. Commun.* 328:342–347.

26. Chen, X., Q. Cui, …, A. Yethiraj. 2008. Gating mechanisms of mechanosensitive channels of large conductance, I: a continuum mechanics-based hierarchical framework. *Biophys. J.* 95:563–580.

27. Goetz, R., G. Gompper, and R. Lipowsky. 1999. Mobility and elasticity of self-assembled membranes. *Phys. Rev. Lett.* 82:221–224.

28. Marcelja, S. 1974. Chain ordering in liquid crystals: II. Structure of bilayer membranes. *Biochim. Biophys. Acta.* 367:165–176.

29. Fattal, D. R., and A. Ben-Shaul. 1993. A molecular model for lipid-protein interaction in membranes: the role of hydrophobic mismatch. *Biophys. J.* 65:1795–1809.

30. Fournier, J. B. 1999. Microscopic membrane elasticity and interactions among membrane inclusions: interplay between the shape, dilation, tilt and tilt-difference modes. *Eur. Phys. J. B.* 11:261–272.

31. May, S., and A. Ben-Shaul. 1999. Molecular theory of lipid-protein interaction and the Lα-HII transition. *Biophys. J.* 76:751–767.

32. Khelashvili, G., S. Mondal, …, H. Weinstein. 2010. Cholesterol modulates the membrane effects and spatial organization of membrane-penetrating ligands for G-protein coupled receptors. *J. Phys. Chem. B.* 114:12046–12057.

33. Partenskii, M. B., and P. C. Jordan. 2002. Membrane deformation and the elastic energy of insertion: perturbation of membrane elastic constants due to peptide insertion. *J. Chem. Phys.* 117:10768–10777.

34. Palczewski, K. 2010. Oligomeric forms of G protein-coupled receptors (GPCRs). *Trends Biochem. Sci.* 35:595–600.

35. Zhou, F. X., M. J. Cocco, …, D. M. Engelman. 2000. Interhelical hydrogen bonding drives strong interactions in membrane proteins. *Nat. Struct. Biol.* 7:154–160.

36. Guo, W., L. Shi, …, J. A. Javitch. 2005. Crosstalk in G protein-coupled receptors: changes at the transmembrane homodimer interface determine activation. *Proc. Natl. Acad. Sci. USA.* 102:17495–17500.

37. Mancia, F., Z. Assur, …, W. A. Hendrickson. 2008. Ligand sensitivity in dimeric associations of the serotonin 5HT2c receptor. *EMBO Rep.* 9:363–369.

38. Fotiadis, D., Y. Liang, …, K. Palczewski. 2003. Atomic-force microscopy: rhodopsin dimers in native disc membranes. *Nature.* 421:127–128.

39. Fotiadis, D., B. Jastrzebska, …, A. Engel. 2006. Structure of the rhodopsin dimer: a working model for G-protein-coupled receptors. *Curr. Opin. Struct. Biol.* 16:252–259.

40. Okada, T., M. Sugihara, …, V. Buss. 2004. The retinal conformation and its environment in rhodopsin in light of a new 2.2 A crystal structure. *J. Mol. Biol.* 342:571–583.

41. Phillips, J. C., R. Braun, …, K. Schulten. 2005. Scalable molecular dynamics with NAMD. *J. Comput. Chem.* 26:1781–1802.

42. Essmann, U., L. Perera, …, L. G. Pedersen. 1995. A smooth particle mesh Ewald method. *J. Chem. Phys.* 103:8577–8593.

43. Martyna, G. J., D. J. Tobias, and M. L. Klein. 1994. Constant pressure molecular dynamics algorithms. *J. Chem. Phys.* 101:4177–4189.

44. Feller, S. E., Y. Zhang, …, B. R. Brooks. 1995. Constant pressure molecular dynamics simulation: the Langevin piston method. *J. Chem. Phys.* 103:4613.

45. Mackerell, Jr., A. D., M. Feig, and C. L. Brooks, 3rd. 2004. Extending the treatment of backbone energetics in protein force fields: limitations of gas-phase quantum mechanics in reproducing protein conformational distributions in molecular dynamics simulations. *J. Comput. Chem.* 25:1400–1415.

46. MacKerell, Jr., A. D., D. Bashford, …, S. Ha. 1998. All-atom empirical potential for molecular modeling and dynamics studies of proteins. *J. Phys. Chem. B.* 102:3586–3616.

47. Pitman, M. C., F. Suits, …, S. E. Feller. 2004. Molecular-level organization of saturated and polyunsaturated fatty acids in a phosphatidylcholine bilayer containing cholesterol. *Biochemistry.* 43:15318–15328.

48. Shan, J., H. Weinstein, and E. L. Mehler. 2010. Probing the structural determinants for the function of intracellular loop 2 in structurally cognate G-protein-coupled receptors. *Biochemistry.* 49:10691–10701.

49. Shi, L., M. Quick, …, J. A. Javitch. 2008. The mechanism of a neurotransmitter:sodium symporter—inward release of Na^+ and substrate is triggered by substrate in a second binding site. *Mol. Cell.* 30:667–677.

50. Chen, Z., and R. P. Rand. 1997. The influence of cholesterol on phospholipid membrane curvature and bending elasticity. *Biophys. J.* 73:267–276.

51. Khelashvili, G., D. Harries, and H. Weinstein. 2009. Modeling membrane deformations and lipid demixing upon protein-membrane interaction: the BAR dimer adsorption. *Biophys. J.* 97:1626–1635.

52. Rawicz, W., K. C. Olbrich, …, E. Evans. 2000. Effect of chain length and unsaturation on elasticity of lipid bilayers. *Biophys. J.* 79:328–339.

53. Bermúdez, H., D. A. Hammer, and D. E. Discher. 2004. Effect of bilayer thickness on membrane bending rigidity. *Langmuir.* 20:540–543.

54. Pan, J., T. T. Mills, …, J. F. Nagle. 2008. Cholesterol perturbs lipid bilayers nonuniversally. *Phys. Rev. Lett.* 100:198103–198106.

55. Elliott, J. R., and D. A. Haydon. 1979. The interaction of n-octanol with black lipid bilayer membranes. *Biochim. Biophys. Acta.* 557:259–263.

56. Chen, G., Z. Li, and P. Lin. 2008. A fast finite difference method for biharmonic equations on irregular domains and its application to an incompressible Stokes flow. *Adv. Comput. Math.* 29:113–133.

57. Ehrlich, L. W. 1971. Solving the biharmonic equation as coupled finite difference equations. *SIAM J. Numer. Anal.* 8:278–287.

58. Smith, J. 1968. The coupled equation approach to the numerical solution of the biharmonic equation by finite differences. I. *SIAM J. Numer. Anal.* 5:323–339.

59. Panaretos, A. H., J. T. Aberle, and R. E. Díaz. 2007. The effect of the 2-D Laplacian operator approximation on the performance of finite-difference time-domain schemes for Maxwell's equations. *J. Comput. Phys.* 227:513–536.

60. Shanno, D. F. 1970. Conditioning of quasi-Newton methods for function minimization. *Math. Comput.* 24:647–656.

61. Lee, B., and F. M. Richards. 1971. The interpretation of protein structures: estimation of static accessibility. *J. Mol. Biol.* 55:379–400, IN373–IN374.

62. Sankararamakrishnan, R., and H. Weinstein. 2002. Positioning and stabilization of dynorphin peptides in membrane bilayers: the mechanistic role of aromatic and basic residues revealed from comparative MD simulations. *J. Phys. Chem. B.* 106:209–218.

63. Yau, W. M., W. C. Wimley, …, S. H. White. 1998. The preference of tryptophan for membrane interfaces. *Biochemistry.* 37:14713–14718.

64. Gray, T. M., and B. W. Matthews. 1984. Intrahelical hydrogen bonding of serine, threonine and cysteine residues within α-helices and its relevance to membrane-bound proteins. *J. Mol. Biol.* 175:75–81.

65. Lindahl, E., and O. Edholm. 2000. Mesoscopic undulations and thickness fluctuations in lipid bilayers from molecular dynamics simulations. *Biophys. J.* 79:426–433.

SUPPORTING MATERIAL

Quantitative modeling of membrane deformations by multi-helical membrane proteins: Application to G-protein Coupled Receptors

Sayan Mondal [†], George Khelashvili [†], Jufang Shan [†], Olaf S. Andersen [†], Harel Weinstein [†,‡]

[†]Department of Physiology and Biophysics, [‡]The HRH Prince Alwaleed Bin Talal Bin Abdulaziz Alsaud Institute for Computational Biomedicine, Weill Medical College of Cornell University

Atomistic molecular dynamics (MD) simulations

All-atom, explicit-solvent MD simulations were carried out on the dark-state structure of monomeric rhodopsin (PDB code 1U19 (1) immersed in fluid lipid bilayers composed of $diC_{14:1}PC$, $diC_{16:1}PC$, $diC_{18:1}PC$, $diC_{20:1}PC$ or a 7:7:6 SDPC/POPC/Chol mixture. We also use the approach presented here in simulations described elsewhere(2) of the $5-HT_{2A}$ serotonin receptor ($5-HT_{2A}R$) monomer in complex with the full agonist 5-HT, the partial agonist LSD and the inverse agonist ketanserin (KET), immersed in the same SDPC/POPC/Chol bilayer.

In all the simulations the protein/lipid molar ratio was ~ 1:350, which is in the range of molar ratios used in FRET experiments investigating the oligomerization of rhodopsin in the same mono-unsaturated PC lipids (3). Our choice of protein concentration also insured that the resulting lipid bilayer patches were large enough to allow the membrane perturbations at the membrane/protein interface to dissipate within the MD box.

All MD simulations were performed with the NAnoscale Molecular Dynamics (NAMD) suite (4), under constant temperature (at 303 K for simulations with mono-unsaturated lipids, and at 310K for simulations with SDPC/POPC/Chol membrane) and pressure (1 atm) conditions with semi-isotropic pressure coupling, and PME for long-range electrostatics (5). The Nose-Hoover Langevin piston method (4, 6, 7) was used to control the target pressure with the LangevinPistonPeriod set to 100 fs and LangevinPistonDecay set to 50 fs. The simulations were performed with rigidBonds allowing 2 fs time step. The CHARMM27 force field (8-10) was used for both proteins and lipids. The $5-HT_{2A}R$ is a homology model based on rhodopsin and β_2AR as templates and its loops were built using the *ab inito* method MC-SCV (11).

All the simulated systems were equilibrated following the procedure described in (12) (also see Figs. S1 and S2). In this protocol, the GPCR backbones and the heavy atoms of the ligand were initially fixed and then harmonically constrained, and water was prevented from penetrating the protein-lipid interface. Constraints were released gradually in four 300 ps steps with decreasing force constants of 1, 0.5, 0.1 and 0.01 $kcal/(mol·Å^2)$, respectively. Following this equilibration phase, each GPCR-membrane complex was simulated for extended period of time. In particular, simulations of rhodospin were carried out for ~250 ns in each membrane model, whereas $5-HT_{2A}R$ simulations in complex with ligands 5-HT, LSD and KET each were conducted for ~350 ns. These timescales were long enough to sample efficiently the ligand-induced conformational changes in the $5-HT_{2A}R$ and concomitant membrane remodeling.

The trajectories were analyzed by: 1) centering each snapshot for the last 100 ns with respect to the center of mass of the protein; 2) fitting a rectangular grid to the positions of the phosphate and C_2 atoms in the two leaflets; and 3) calculating the time-averaged phosphate-phosphate and C_2-C_2 bilayer thickness on the rectangular grid (grid spacing 2 Å), which is then converted to a deformation profile using Eq. 1 in the main text. The MD deformation profile, such as in Fig. 1A, is then smoothed by spatial averaging. For the purpose of defining the membrane boundary near the protein, a grid square was considered populated by lipid if during the trajectory it was visited by the phosphate atoms in both leaflets.

Parametrization of the continuum model

For the continuum (CT) formulation, the following inputs were obtained from the cognate MD trajectories: the protein/lipid boundary contour Γ_{in}, the membrane thickness u_0 at this boundary, the outer boundary contour Γ_{out} of the MD box, and the average membrane thickness d_0 at Γ_{out}. These inputs were obtained from the MD phosphate-phosphate deformation profile (e.g., Fig. 1 for rhodopsin in diC$_{14:1}$PC).

The CT formulation requires several empirical parameters that were estimated from experimental measurements described in the literature. In particular, the spontaneous curvature C_0 for the diC$_{14:1}$PC, diC$_{16:1}$PC, diC$_{18:1}$PC, diC$_{20:1}$PC and POPC lipids were taken to be 0 Å^{-1}, based on near-cylindrical shape of these lipids. For the SDPC/POPC/Chol mixture, C_0 was taken to be $\sim$ -0.015 Å^{-1}, based on the relation (13, 14)

$$C_0^{SDPC/POPC/Chol} = \mu_{chol}C_{0,chol} + \mu_{POPC}C_{0,POPC} + \mu_{SDPC}C_{0,SDPC}, \quad (S1)$$

where $\mu_{chol} = 0.35$, $\mu_{POPC} = 0.35$ and $\mu_{SDPC} = 0.3$ are the mole fractions and $C_{0,chol}$, $C_{0,POPC}$ and $C_{0,SDPC}$ the spontaneous curvatures of cholesterol, POPC, and SDPC respectively. Based on experimental estimates, we have used $C_{0,chol} = $ -0.04 Å^{-1}(13, 15). Measurements are not available for $C_{0,SDPC}$, and we used the spontaneous curvature value of DOPC, -0.011 Å^{-1}, based on the experimental observation that C_0 for SDPE and DOPE are similar (16).

The compressibility modulus K_a was taken to be 230 mN/m for all the membranes (17); for the bending modulus K_c of diC$_{18:1}$PC we used 0.9×10^{-19} J (22 k_BT) (17). This value then was used to infer the K_c for the other monounsaturated PC membranes using the relation $K_c \propto K_a d_0^2$ (18). K_c is known to decrease with unsaturation and was taken to be 0.4×10^{-19} J for the SDPC/POPC/Chol membranes, because of the polyunsaturated docosahexaenoyl chain in SDPC lipid. We did not consider any additional effect of cholesterol on K_a or K_c of the SDPC/POPC/cholesterol membranes. Cholesterol has been shown to have only small effects on the elastic parameters of bilayers with unsaturated acyl chains (19) and, given the high unsaturation of SDPC, can be expected to not substantially affect the K_a or K_c of these mixtures. The surface tension α was taken to be 3×10^{-3} N/ Å (20, 21).

Solution of the Euler-Lagrange equation (Eq. 4)

To solve the boundary value problem in Eq. 4 without introducing the simplifying assumption of radial symmetry, we converted the fourth order differential in $u(x,y)$ to a couple of simultaneous second order equations in u and v (22-24):

$$K_c\nabla^2 v - \alpha v + \frac{4K_a}{d_0^2}u = 0,$$

$$\nabla^2 u = v, \quad (S2)$$

$$u|_{\Gamma in} = u_o(x,y), u|_{\Gamma out} = u_1(x,y), v|_{\Gamma in} = v_0(x,y), v|_{\Gamma out} = v_1(x,y)$$

This set of equations was solved numerically for $u(x,y)$ on a rectangular grid using a standard finite difference scheme for Poisson equations. Specifically, Eq. S2 was discretized using the central 5-point approximation of the Laplacian operator (25), and the system was then solved using the iterative Gauss-Siedel algorithm, which in our case typically takes 125-150 iterations to converge.

The boundary condition $v_0(x,y)$ was obtained self-consistently using an optimization procedure to search for $v_0(x,y)$ that would globally minimize ΔG_{def} (see Theory and Methods section). To reduce the complexity of the optimization problem, $v_0(x,y)$ was first expressed as a truncated Fourier series,

$$v_o(x,y) : v_0(\theta) \sim \sum_{n=0}^{7} \{a_n \cos(n\theta) + b_n \sin(n\theta)\}, \text{ (S3)}$$

where θ is the polar angle corresponding to the coordinates (x,y), and a_n and b_n are the Fourier coefficients. Then, for any given $\{a_n, b_n\}$, Eq. S2 gives the membrane deformation profile, and Eq. 2 the corresponding ΔG_{def}. We solved the non-linear optimization problem with the objective function $\Delta G_{def} = f\{a_n, b_n\}$ using the BFGS optimization algorithm (26), which is a global, quasi-Newtonian optimization procedure. Every optimization calculation is performed in three replicates, starting with a random seed.

The boundary condition $v_0(x,y)$ used here is the asymmetric generalization of the so-called natural boundary condition (27). Other choices, e.g. using the slope rather than the curvature at the protein/bilayer boundary, can also be implemented.

The usual assumption of radial symmetry leads to an underestimation of the membrane deformation energy. For rhodopsin in diC$_{14:1}$PC, we calculated the membrane deformation energy using the CTMD formalism presented here for asymmetric proteins, but setting the membrane deformation at all points on the protein-membrane boundary uniformly to the value of the average membrane deformation near the protein, and compared to the value obtained using the 1D CTMD algorithm used in (15), which can be applied in the radially symmetric case. These calculations, predicated on the assumption of radial symmetry, yielded ~1.9 kT (the 1D CTMD has ~0.5 kT uncertainty due to choosing a single diameter to represent the irregular protein-membrane boundary), which should be contrasted with the 4.7 kT obtained when not making the assumption of radial symmetry.

Calculation of the Energy Penalty due to Residual Exposure at the *ith* TM segment ($\Delta G_{res,i}$)

The energy penalty $\Delta G_{res,i}$ penalizes hydrophilic residues of the protein exposed to the hydrophobic core of the lipid environment as well as hydrophobic residues of the protein exposed to polar environment. It is calculated according to Eq. 3 in the main text. Here we describe the procedure to calculate the residual exposure in more detail.

To obtain the residual exposure $SA_{res,i}$ at the ith TM segment in Eq. 3, we calculated first the local membrane thickness $L_{m,i}$ near the ith TM segment as the average membrane thickness in

a circular sector spanning that TM segment and within a 12 Å cutoff of the C_α atoms of the TM segment, as illustrated in Figs. S4 and S5.

If the hydrophobic length L_i of the TM segment along the Z-axis exceeds that of the surrounding membrane ($L_i > L_{m,i}$), the hydrophobic residues of the protein exposed to polar environment are identified directly. Therefore, for these residues, we need to calculate the surface area that is not facing the hydrophobic core of the lipid membrane or the protein, but is instead exposed to polar environment. Therefore, $SA_{res,i}$ is calculated as the total SASA (SASA obtained with the standard algorithm of Lee & Richards (29) implemented in the software NACCESS, http://www.bioinf.manchester.ac.uk/naccess/) of these residues with the solute being the entire protein and hydrophobic part of the bilayer. For convenience, we will refer to this as: SASA {solute=protein+hydrophobic part of the membrane}

If $L_i < L_{m,i}$, the hydrophilic residues of the protein exposed to hydrophobic environment are identified, and $SA_{res,i}$ for this TM segment is obtained as SASA {solute=protein} – SASA {solute=protein+hydrophobic part of the membrane}. In this case, we subtract the term SASA {solute=protein+hydrophobic part of the membrane} to eliminate partial exposure of these hydrophilic residues to the polar part of the bilayer.   The computed $SA_{res,i}$ is then used to obtain the residual exposure energy according to Eq. 3.

For these calculations, interfacial lysine and arginine residues were considered not to contribute to the hydrophobic mismatch due to the expected snorkeling effect (30). Interfacial tryptophan was also not considered to add to hydrophobic mismatch penalty. Although tryptophan may be classified as a hydrophobic residue, it favors interfacial location (31). In addition, serine and threonine residue are polar residues, but when they reside within the hydrophobic part of the membrane, their polar parts can form H-bonds with the helix backbone (32). Therefore, serine and threonine were also ignored for the residual exposure calculations.

TABLES

Table S1 Comparison of the bilayer thickness d_0 at the outer boundary of the simulation box and near the protein (within 12 Å) and the energy penalty ΔG_{def} for the protein-induced membrane deformations

System	d_0 (Å)	Average thickness near the protein (Å)	delta (Å)	ΔG_{def} (kT)
Rhodopsin-diC$_{14:1}$PC	33.4	35.8	2.2	4.7
Rhodopsin-diC16:1PC	37.0	38.2	1.2	1.6
Rhodopsin-diC18:1PC	41.6	41.6	0	<1
Rhodopsin-diC20:1P	46.7	45.4	-1.3	2
Rhodopsin-SDPC/POPC/Chol	49.5*	47.0	-2.5	2.6
5HT$_{2A}$R- 5HT-	49.5*	48.1	-1.4	<1

SDPC/POPC/Chol				
5HT$_{2A}$R- KET-SDPC/POPC/Chol	49.5*	47.7	-1.8	<1
5HT$_{2A}$R- LSD-SDPC/POPC/Chol	49.5*	48.7	-0.84	<1

*d_0 for SDPC/POPC/Chol is the average for the four systems

Table S2 Comparison of membrane thickness L_m near each TM segment of rhodopsin in different membranes and the hydrophobic length L_i of the TM[a]

TM	diC$_{14:1}$PC		diC$_{16:1}$PC		diC$_{18:1}$PC		diC$_{20:1}$PC		SDPC/POPC/Chol	
	$L_{m,i}$ (Å)	L_i (Å)	$L_{m,i}$ (Å)	L_i (Å)	$L_{m,i}$ (Å)	L_i (Å)	$L_{m,i}$ (Å)	L_i (Å)	$L_{m,i}$ (Å)	L_i (Å)
1	28.8	37.0	31.6	36.7	33.5	37.0	39.9	37.7	40.4	39.7
2	29.4	35.8	32.3	33.0	33.4	34.8	39.3	34.7	39.8	34.1
4	31.5	29.0	30.9	29.4	34.8	28.9	37.6	29.2	41.2	29.1
5	29.8	31.0	31.9	31.5	34.5	32.0	37.8	30.7	39.8	29.4
6	28.8	34.7	30.9	35.9	33.6	36.5	35.1	36.4	37.9	36.7
7	29.0	36.9	32.5	37.6	34.1	37.8	37.6	37.8	36.3	37.6

a) using the following TM definitions (given in the Ballesteros-Weinstein generic numbering (33)): 1.29–1.59 (TM1), 2.38–2.66 (TM2), 4.43–4.62 (TM4), 5.38–5.63 (TM5), 6.33–6.59 (TM6), 7.32–7.56 (TM7)

Table S3 Comparison of membrane thickness L_m near each TM segment of 5-HT$_{2A}$R in complex with agonist (5-HT), partial agonist (LSD) and inverse agonist (KET) respectively and the hydrophobic length L_i of the TM segment[a]

TM	5-HT$_{2A}$R with 5-HT		5-HT$_{2A}$R with LSD		5-HT$_{2A}$R with KET	
	$L_{m,i}$(Å)	L_i (Å)	$L_{m,i}$(Å)	L_i (Å)	$L_{m,i}$(Å)	L_i (Å)
1	43.0	41.0	45.2	43.3	40.8	41.3
2	43.1	37.9	44.0	39.8	40.1	40.5
4	41.4	36.6	42.9	35.3	42.2	34.9
5	42.8	33.9	41.3	32.8	41.5	33.3
6	42.8	37.9	42.3	37.0	43.6	36.8
7	41.5	36.1	42.7	36.9	42.0	38.0

a) using the following TM definitions (given in the Ballesteros-Weinstein generic numbering (33)): 1.29–1.59 (TM1), 2.38–2.67 (TM2), 4.39–4.63 (TM4), 5.38–5.63 (TM5), 6.33–6.59 (TM6), 7.30–7.56 (TM7)
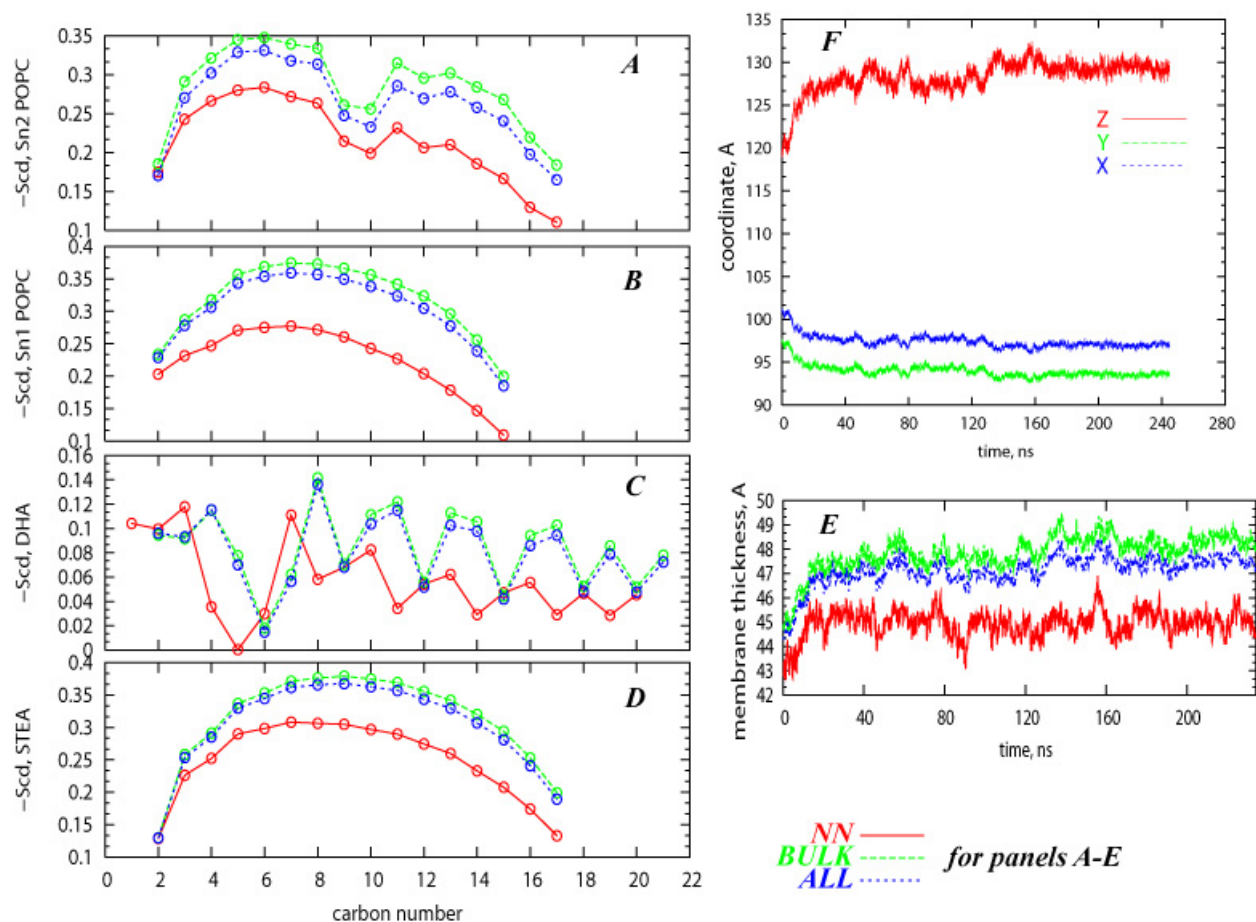
SUPPORTING FIGURES

FIGURE S1 Structural parameters of the 7:7:6 SDPC/POPC/Chol membrane around rhodopsin. (*A-D*) The values of carbon deuterium order parameters, -S_{CD} for POPC sn2 (*A*) and sn1 (*B*) tails, and for DHA (*C*) and STEA (*D*) chains on the SDPC lipid. The three plots in each panel correspond to calculations for all the lipids in the system (*blue*), for the lipids within 10 Å of the protein (*red*), and for the lipids 10 Å away from the protein (*green*). (*E*) Membrane thickness as a function of time, measured from the average phosphate-to-phosphate distances on the two leaflets of the bilayer. Shown are profiles for the entire membrane (*blue*), for the membrane region within 10 Å of the protein (*red*), and for the membrane patch outside the 10Å shell around the protein (*green*). (*F*) Time evolution of the box *X* (*blue*), *Y* (*green*), and *Z* (*red*) dimensions.
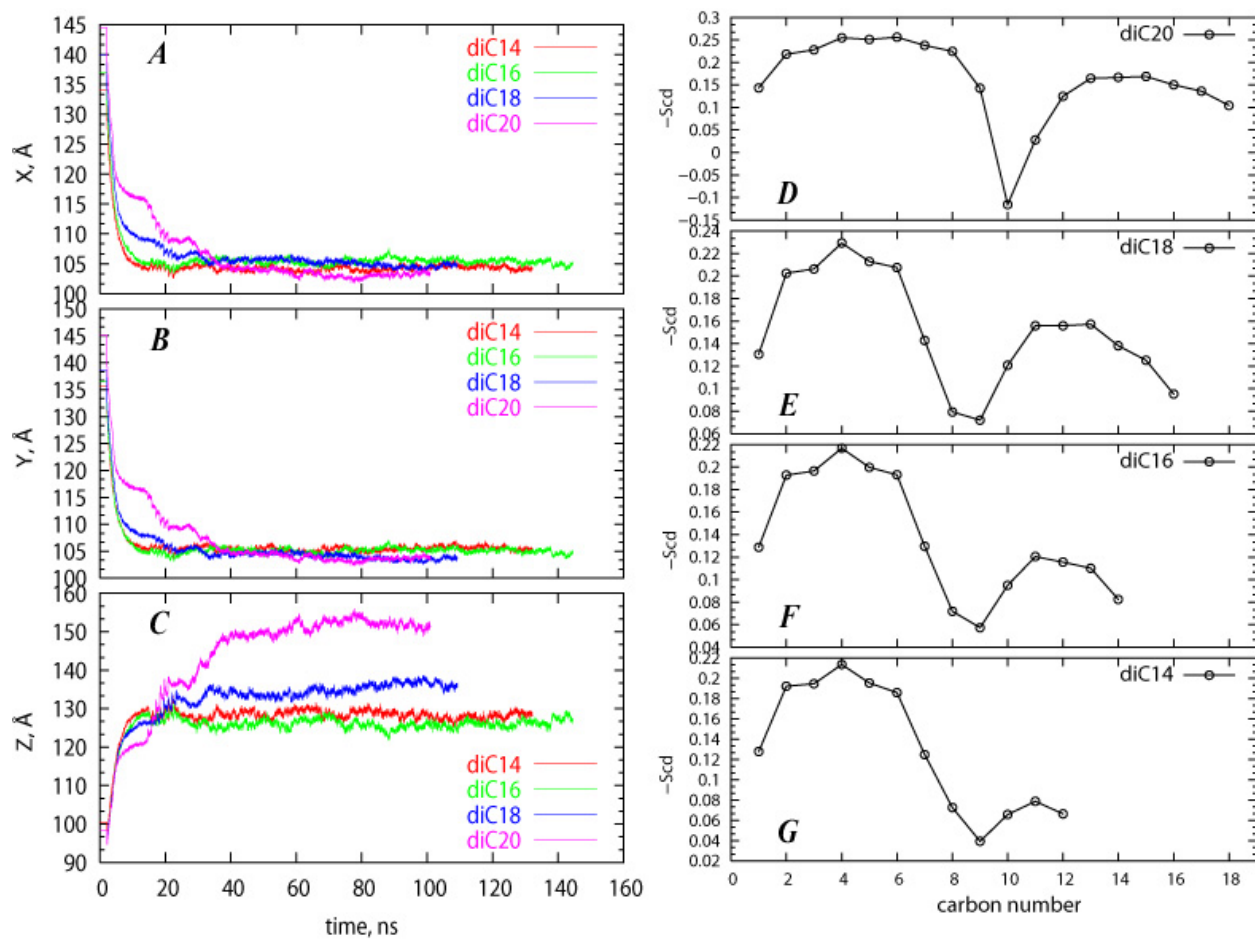
FIGURE S2 (*A-C*) Equilibration of the box dimensions in the MD trajectories of rhodopsin in diC$_{14:1}$PC (blue), diC$_{16:1}$PC (cyan), diC$_{18:1}$PC (green), and diC$_{20:1}$PC (magenta). The first 40 ns of each trajectory were discarded from the analysis presented in the manuscript. (*D-G*) The values of carbon deuterium order parameters, -S_{CD} for diC$_{14:1}$PC (*D)*, diC$_{16:1}$PC (*E*), diC$_{18:1}$PC (*F*), and diC$_{20:1}$PC (*G*) lipids.
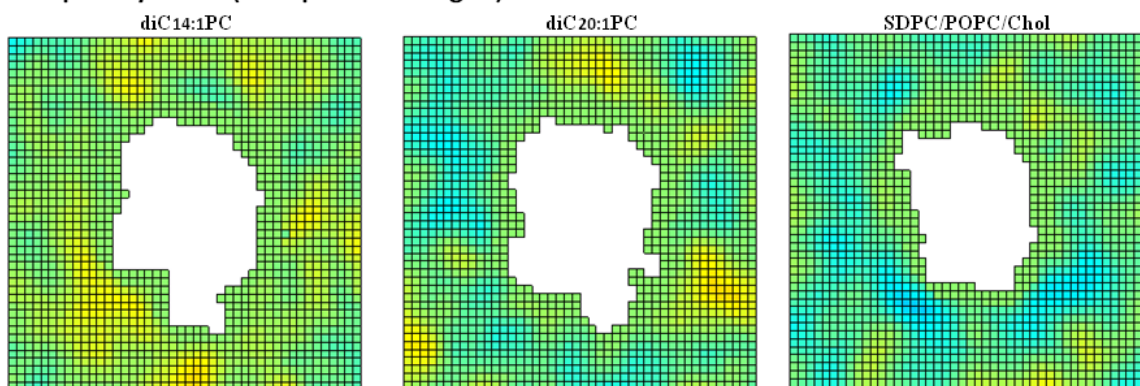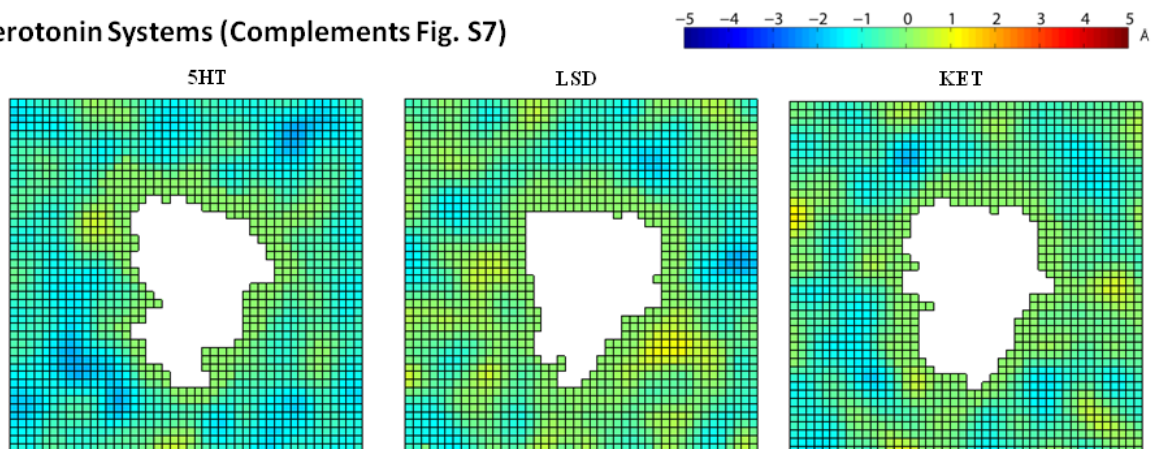
FIGURE S3 Colormaps for $u_{CTMD}(x,y)$-$u_{MD}(x,y)$ showing the difference between the membrane deformation profile $u_{CTMD}(x,y)$ obtained from CTMD and $u_{MD}(x,y)$ obtained directly from MD. These maps complement the membrane shapes shown in Fig. 2 and Fig. S7 below. The range of differences between $u_{MD}(x,y)$ and $u_{CTMD}(x,y)$ is only 0-2 Å, which is within the 2-3 Å RMS amplitude of the fluctuations expected in bilayers of length scale ~100 Å (34).

FIGURE S4 Angular segments (*red points*) used to associate membrane grid points (*black dots*) with each TM segment for calculating the membrane thickness near that helix, illustrated for rhodopsin in $diC_{14:1}PC$ membrane. For completeness, the average structure of the receptor (*cartoon*) is also shown to illustrate the approximate positions and orientations of each TM segment (*numbered and colored*). For these calculations, the grid points in each segment were selected to be within 12 Å distance from the C_α atoms of the TM segment and within the angular region encompassing the span of the TM segment.
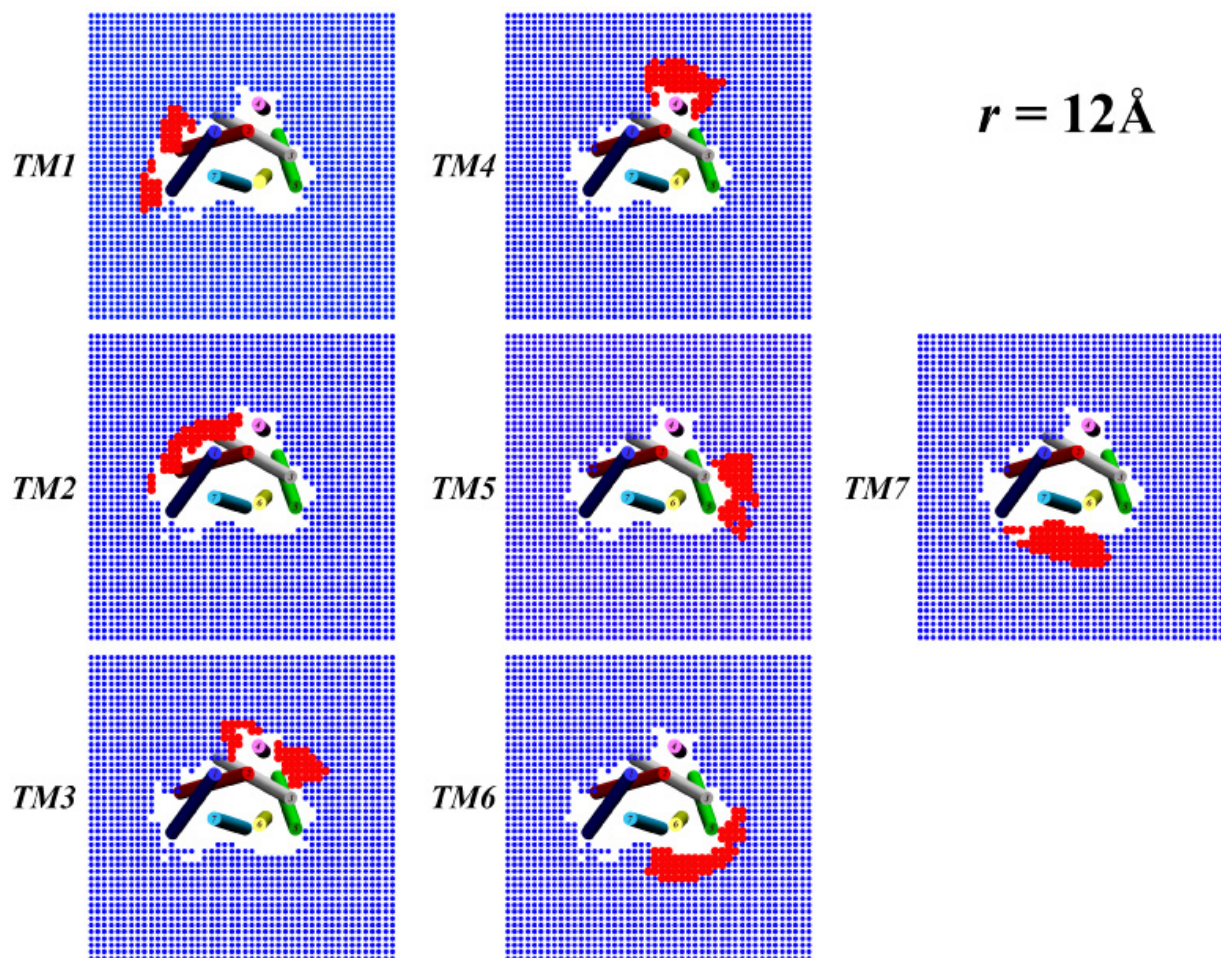
FIGURE S5 Angular segments (*red points*) used to associate membrane grid points (*points in blue*) with each TM segment for calculating the membrane thickness near that helix, illustrated for 5HT-bound 5-HT$_{2A}$R in 7:7:6 SDPC/POPC/Cholesterol membrane. For completeness, the average structure of the receptor (*cartoon*) is also shown to illustrate the approximate positions and orientations of each TM segment (*numbered and colored*). For these calculations, the grid points in each segment were selected to be within 12 Å distance from the C$_\alpha$ atoms of the TM segment and within the angular region encompassing the span of the TM segment.
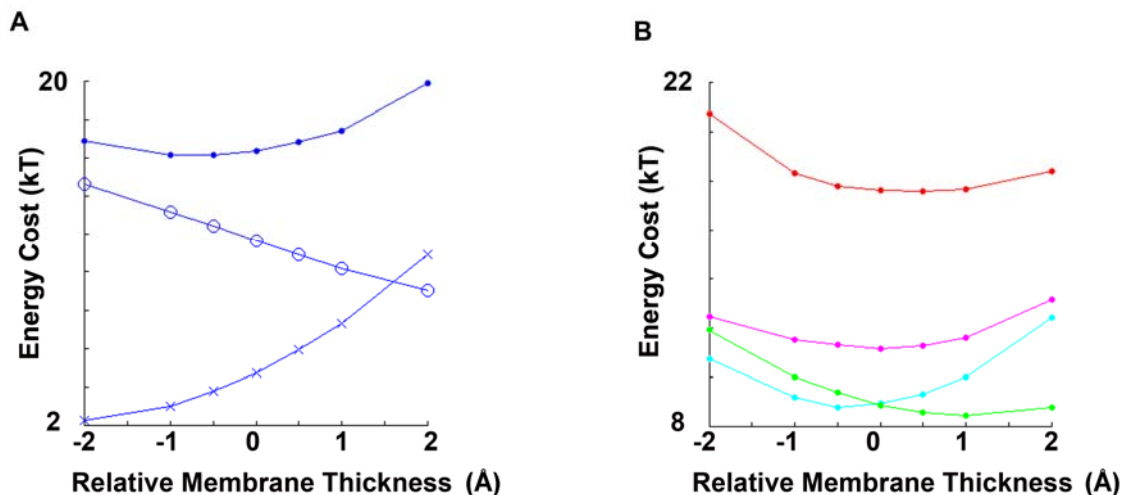
FIGURE S6 The energy cost due to hydrophobic mismatch as a function of the membrane thickness at the membrane-protein interface, the membrane thickness being expressed relative to that obtained from MD. Along the X-axis, X=0 corresponds to the thickness at the membrane-protein boundary from MD, and increasing thickness indicates increasing membrane deformation at the interface. Note that the changes in the membrane thickness along the X-axis were done keeping the pattern of membrane deformations at membrane-protein interface from MD, i.e., membrane thickness was changed by the same magnitude at all points on the membrane-protein interface. (A) The total energy cost and its components for rhodopsin in $diC_{14:1}PC$. The data points for the membrane deformation component are denoted by crosses (x), the residual exposure component by open circles (o), and the total energy cost by dots (.) (B) The total energy cost for rhodopsin in $diC_{16:1}PC$ (cyan), $diC_{18:1}PC$ (green), $diC_{20:1}PC$ (magenta) and SDPC/POPC/cholesterol (red). For this numerical experiment, the residual exposure area was determined at each data point from the residual exposure (L_m-L_i) and the perimeter of the TM segment-lipid interface (as in Fig. S4), done as in ref. (35).
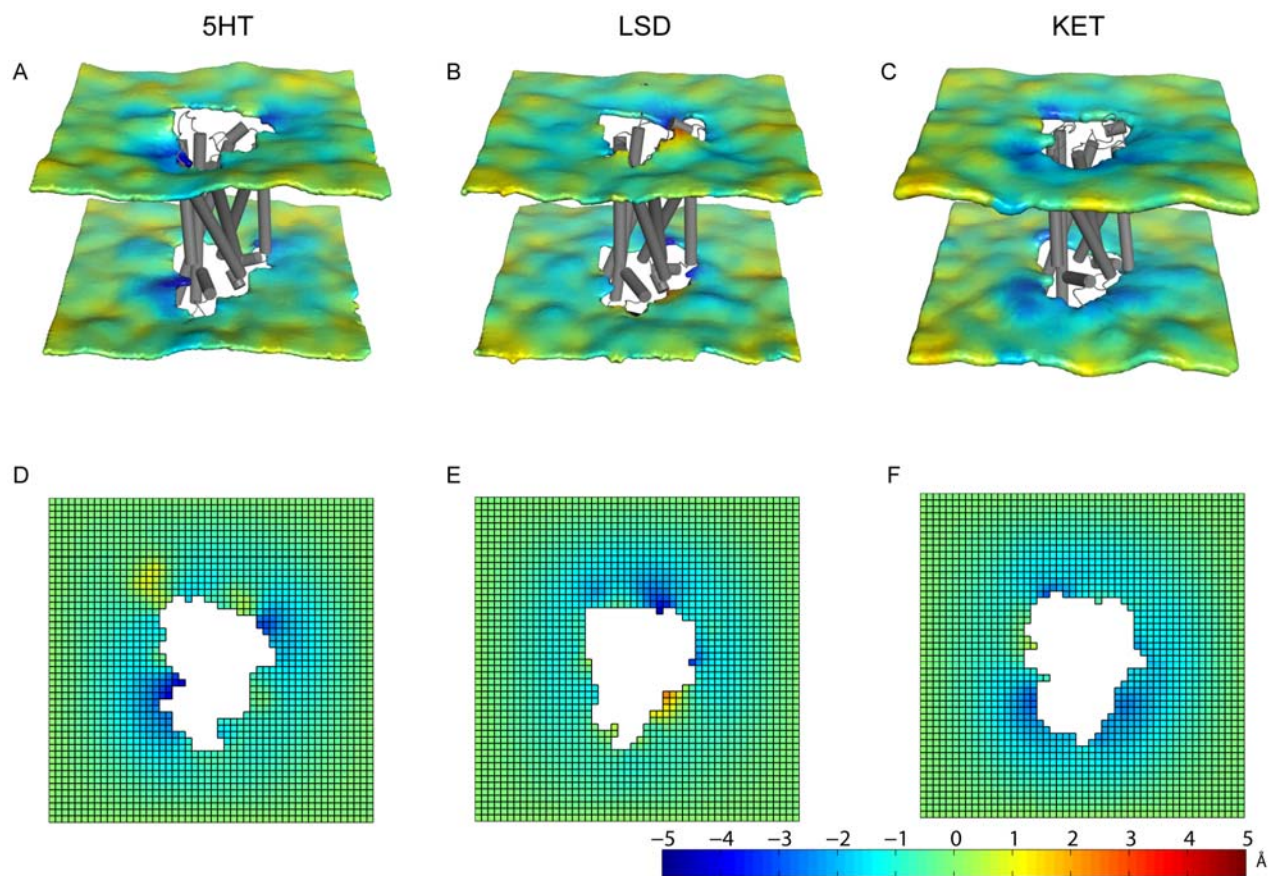
FIGURE S7 Membrane deformation profiles $u(x,y)$ for ligand-bound 5-HT$_{2A}$R in native-like 7:7:6 SDPC/POPC/cholesterol bilayers. The upper panel shows $u(x,y)$ calculated directly from the MD trajectories for three different conformations of the receptor-ligand complex: (*A*) with the full agonist (*5-HT*); (*B*) with the partial agonist (*LSD*); and (*C*) with the inverse agonist (*KET*). The lower panel shows the corresponding $u(x,y)$ from 3D-CTMD calculations for (*D*) 5-HT; (*E*) LSD; and (*F*) KET. $\Delta G_{def} < 1$ $k_B T$ in all cases.

REFERENCES

1. Okada, T., M. Sugihara, A. N. Bondar, M. Elstner, P. Entel, and V. Buss. 2004. The Retinal Conformation and its Environment in Rhodopsin in Light of a New 2.2 Å Crystal Structure+. J. Mol. Biol. 342:571-583.
2. Shan, J., G. Khelashvili, S. Mondal, and H. Weinstein. 2011. Pharmacologically Distinct Ligands Induce Different States of 5-HT2AR and Trigger Different Membrane Remodeling: Implications For GPCR Oligomerization. Biophys. J. 100:254.
3. Botelho, A. V., T. Huber, T. P. Sakmar, and M. F. Brown. 2006. Curvature and hydrophobic forces drive oligomerization and modulate activity of rhodopsin in membranes. Biophys. J. 91:4464-4477.
4. Phillips, J. C., R. Braun, W. Wang, J. Gumbart, E. Tajkhorshid, E. Villa, C. Chipot, R. D. Skeel, L. Kale, and K. Schulten. 2005. Scalable molecular dynamics with NAMD. Journal of computational chemistry 26:1781.
5. Essmann, U., L. Perera, M. L. Berkowitz, T. Darden, H. Lee, and L. G. Pedersen. 1995. A smooth particle mesh Ewald method. Journal of Chemical Physics 103:8577-8593.
6. Martyna, G. J., D. J. Tobias, and M. L. Klein. 1994. Constant pressure molecular dynamics algorithms. constraints 101:4177-4189.
7. Feller, S. E., Y. Zhang, R. W. Pastor, and B. R. Brooks. 1995. Constant pressure molecular dynamics simulation: the Langevin piston method. The Journal of chemical physics 103:4613.
8. MacKerell, A. D., M. Feig, and C. L. Brooks. 2004. Extending the treatment of backbone energetics in protein force fields: limitations of gas-phase quantum mechanics in reproducing protein conformational distributions in molecular dynamics simulations. Journal of computational chemistry 25:1400-1415.
9. MacKerell Jr, A. D., D. Bashford, M. Bellott, R. L. Dunbrack Jr, J. D. Evanseck, M. J. Field, S. Fischer, J. Gao, H. Guo, and S. Ha. 1998. All-atom empirical potential for molecular modeling and dynamics studies of proteins. The Journal of Physical Chemistry B 102:3586-3616.
10. Pitman, M. C., F. Suits, A. D. MacKerell Jr, and S. E. Feller. 2004. Molecular-level organization of saturated and polyunsaturated fatty acids in a phosphatidylcholine bilayer containing cholesterol. Biochemistry 43:15318-15328.
11. Shan, J., H. Weinstein, and E. L. Mehler. Probing the Structural Determinants for the Function of Intracellular Loop 2 in Structurally Cognate G-Protein-Coupled Receptors. Biochemistry 49:10691-10701.
12. Shi, L., M. Quick, Y. Zhao, H. Weinstein, and J. A. Javitch. 2008. The mechanism of a neurotransmitter: sodium symporter--inward release of Na+ and substrate is triggered by substrate in a second binding site. Mol. Cell 30:667-677.
13. Chen, Z., and R. P. Rand. 1997. The influence of cholesterol on phospholipid membrane curvature and bending elasticity. Biophys. J. 73:267-276.
14. Khelashvili, G., D. Harries, and H. Weinstein. 2009. Modeling Membrane Deformations and Lipid Demixing upon Protein-Membrane Interaction: The BAR Dimer Adsorption. Biophys. J. 97:1626-1635.
15. Khelashvili, G., S. Mondal, O. S. Andersen, and H. Weinstein. 2010. Cholesterol Modulates the Membrane Effects and Spatial Organization of Membrane-Penetrating

Ligands for G-Protein Coupled Receptors. The Journal of Physical Chemistry B 114:12046-12057.

16. Soubias, O., W. E. Teague Jr, K. G. Hines, D. C. Mitchell, and K. Gawrisch. 2010. Contribution of Membrane Elastic Energy to Rhodopsin Function. Biophys. J. 99:817-824.

17. Rawicz, W., K. C. Olbrich, T. McIntosh, D. Needham, and E. Evans. 2000. Effect of chain length and unsaturation on elasticity of lipid bilayers. Biophys. J. 79:328-339.

18. Bermudez, H., D. A. Hammer, and D. E. Discher. 2004. Effect of bilayer thickness on membrane bending rigidity. Langmuir 20:540-543.

19. Pan, J., T. T. Mills, S. Tristram-Nagle, and J. F. Nagle. 2008. Cholesterol perturbs lipid bilayers nonuniversally. Physical Review Letters 100:198103-198106.

20. Elliott, J. R., and D. A. Haydon. 1979. The interaction of n-octanol with black lipid bilayer membranes. Biochimica et Biophysica Acta (BBA)-Biomembranes 557:259-263.

21. Nielsen, C., M. Goulian, and O. S. Andersen. 1998. Energetics of inclusion-induced bilayer deformations. Biophys. J. 74:1966-1983.

22. Chen, G., Z. Li, and P. Lin. 2008. A fast finite difference method for biharmonic equations on irregular domains and its application to an incompressible Stokes flow. Advances in Computational Mathematics 29:113-133.

23. Ehrlich, L. W. 1971. Solving the biharmonic equation as coupled finite difference equations. SIAM Journal on Numerical Analysis 8:278-287.

24. Smith, J. 1968. The coupled equation approach to the numerical solution of the biharmonic equation by finite differences. I. SIAM Journal on Numerical Analysis:323-339.

25. Panaretos, A. H., J. T. Aberle, and R. E. Díaz. 2007. The effect of the 2-D Laplacian operator approximation on the performance of finite-difference time-domain schemes for Maxwell's equations. Journal of Computational Physics 227:513-536.

26. Shanno, D. F. 1970. Conditioning of quasi-Newton methods for function minimization. Mathematics of Computation 24:647-656.

27. Aranda-Espinoza, H., A. Berman, N. Dan, P. Pincus, and S. Safran. 1996. Interaction between inclusions embedded in membranes. Biophys. J. 71:648-656.

28. West, B., F. L. H. Brown, and F. Schmid. 2009. Membrane-protein interactions in a generic coarse-grained model for lipid bilayers. Biophys. J. 96:101-115.

29. Lee, B., and F. M. Richards. 1971. The interpretation of protein structures: estimation of static accessibility. J. Mol. Biol. 55:379-400, IN373-IN374.

30. Sankararamakrishnan, R., and H. Weinstein. 2002. Positioning and stabilization of dynorphin peptides in membrane bilayers: the mechanistic role of aromatic and basic residues revealed from comparative MD simulations. J. Phys. Chem. B 106:209-218.

31. Yau, W. M., W. C. Wimley, K. Gawrisch, and S. H. White. 1998. The preference of tryptophan for membrane interfaces. Biochemistry 37:14713-14718.

32. Gray, T. M., and B. W. Matthews. 1984. Intrahelical hydrogen bonding of serine, threonine and cysteine residues within [alpha]-helices and its relevance to membrane-bound proteins* 1. J. Mol. Biol. 175:75-81.

33. Ballesteros, J. A., and H. Weinstein. 1995. Integrated methods for the construction of three-dimensional models and computational probing of structure-function relations in G protein-coupled receptors. In Methods in Neurosciences. Academic Press. 366-428.

34. Lindahl, E., and O. Edholm. 2000. Mesoscopic undulations and thickness fluctuations in lipid bilayers from molecular dynamics simulations. Biophys. J. 79:426-433.
35. Marsh, D. 2008. Energetics of hydrophobic matching in lipid-protein interactions. Biophys. J. 94:3996-4013.